GAIN CHARACTERISTICS IN OPTICALLY-PUMPED CO_2

GAIN CHARACTERISTICS IN OPTICALLY-PUMPED CO_2

By

RAYMOND CHE YIN AUYEUNG, B.Sc.

A thesis

Submitted to the School of Graduate Studies

in Partial Fulfilment of the Requirements

for the Degree

Master of Science

McMaster University

December 1986

MASTER OF SCIENCE (1986)
(PHYSICS)

McMASTER UNIVERSITY
Hamilton, Ontario

TITLE : Gain Characteristics in Optically-Pumped CO_2

AUTHOR: Raymond Che Yin Auyeung, B.Sc. (University of Toronto)

SUPERVISOR: Professor J. Reid

NUMBER OF PAGES: xi, 69

ABSTRACT

Optical pumping at 4.3 μm is used to create high gain coefficients and high vibrational temperatures in the asymmetric (ν_3) mode of CO_2. A pulsed 4.3 μm CO_2 laser excites mixtures of CO_2 and He to create transient gain at 9 and 10 μm. A conventional cw CO_2 laser operating on both regular and sequence bands measures this transient gain and thus determines the ν_3 mode vibrational temperature T_3. The measured values of T_3 are generally much higher than those attained in discharge-excited CO_2. It is shown that a Treanor distribution must be used to describe the populations in the ν_3 mode when dilute mixtures of CO_2 in He are optically pumped to ν_3 mode temperatures of 3000 to 4000 K. Under these conditions, the measured sequence band gain coefficients are almost equal to those on the regular bands. The collisional relaxation of energy from the ν_3 mode shows evidence of fast V-T relaxation at high values of T_3, followed by a slower relaxation rate characteristic of the 00°1 population lifetime. Attempts to create lasing by utilizing the partial inversion predicted in high-lying ν_3 band levels were unsuccessful.

In mixtures with high CO_2 content, 10 μm gain coefficients as large as 20 %/cm on the regular bands and 5 %/cm on the sequence bands have been measured. The high values of gain coefficient and T_3 observed in the optically-pumped system are attributed to the absence of electron

de-excitation mechanisms which limit the excitation of the ν_3 mode in discharge-excited CO_2.

ACKNOWLEDGEMENTS

I would like to thank my supervisor, Dr. J. Reid, for the opportunity of working with him and for his expert guidance in this work.

My sincere thanks are also due to Dr. R.K. Brimacombe for his development of the CO_2 gain models and for introducing me to CO_2 laser research. I am grateful to Messrs. David Danagher and Ed Williams for their development of the data acquisition and analysis programs and to Mr. T. Manuccia for his critical comments of this manuscript.

Lastly but not least, I wish to thank my parents for their constant encouragement and support throughout the course of this work.

CONTENTS

PAGE

LIST OF FIGURES

LIST OF TABLES

Chapter 1

INTRODUCTION

It has long been recognized that CO_2 lasers are one of the most powerful, efficient and versatile sources of coherent radiation in the mid-infrared. Their ease of construction and operation have seen their rise in use in industry, medicine and science. Conventional continuous wave (cw) and pulsed CO_2 lasers operate on the (00°1-02°0) and (00°1-10°0) vib-rotational bands centered at 9.4 and 10.4 μm respectively. Many different methods have been used to excite the CO_2 laser medium, but the most common technique involves a pulsed or cw electric discharge. In recent years, the properties of the gain medium have been well characterized [1,2] and it is generally accepted that CO_2 laser dynamics are best described by a mode-temperature model [1-4]. The most important mode temperature in CO_2 is that of the asymmetric stretching (ν_3) mode, as T_3 controls the population of the upper laser level 00°1. The populations of the lower levels are determined by the combined symmetric stretching (ν_1) and bending (ν_2) mode temperature (T_1 is usually taken as equal to T_2), which is generally within 50 K of the gas kinetic temperature T [5].

As the small-signal gain in the 10 μm laser bands increases with increasing T_3, much effort has gone into maximizing T_3 in electrically-excited CO_2 lasers [5,6]. Calculations indicate that gain coefficients

of > 10 %/cm should be attainable at 10.6 μm [7]. However, the maximum gain coefficients observed in laser discharges are typically ~ 3 %/cm, with ~ 5 %/cm occasionally reported in conventional TE electron-beam systems [8]. This gain limitation is often attributed to electron de-excitation of the ν_3 mode, which results in a saturation of T_3 with increasing input energy [5,7,9,10], but other explanations have been reported [11,12]. It appears that there is some fundamental limitation to T_3 in electrically-excited CO_2 mixtures and in the experiments described in this study, we set out to determine if a similar limitation exists in optically-pumped CO_2.

Optical pumping is a powerful technique for exploring the gain dynamics of any media. Its highly selective nature usually allows one to separate the primary characteristics of a system from secondary effects such as dissociation, thermal heating, differential excitations, etc. In the past, optical pumping of CO_2 has been used extensively to create gain in high-pressure gas mixtures [13], but to date, no detailed measurements have been reported of small-signal gain coefficients in optically-pumped CO_2 systems. In the current series of experiments, a pulsed 4.3 μm CO_2 laser is used to pump mixtures of CO_2 and He, and a cw 10 μm CO_2 laser probes the transient 10 μm gain created by the 4.3 μm pulse. The 4.3 μm source is an ideal pump for CO_2 as the absorbed energy is very efficiently coupled into the ν_3 mode. Measurements are made on both regular and sequence 10 μm transitions to directly determine T_3 [1,7]. Mixtures ranging from 1% CO_2 in He to pure CO_2 at pressures from 300 to 1000 Torr have been investigated. In all cases,

ν_3 mode temperatures much higher than those attained in electric discharges are observed and no evidence is seen of any saturation of T_3 with increasing pump energy. Gain coefficients ranging from 10 to 20 %/cm on the 10 μm band have been measured in high concentration mixtures and T_3 values of ~ 4200 K have been observed in low concentration mixtures. For such high values of T_3, the anharmonicity of the CO_2 molecule must be explicitly taken into account and the vibrational populations of the ν_3 mode treated as a Treanor [14,15] rather than a Boltzmann distribution.

The results in this study is a further indication that electron de-excitation of the ν_3 mode of CO_2 imposes severe limitations on the performance of discharge-excited CO_2 lasers. These limitations can be overcome in an optically-pumped system, but this type of system will only be practical when a more suitable pump source becomes available.

Chapter 2

CO_2 LASER THEORY*

2.1 Introduction

This chapter provides an overview of the gain dynamics of the CO_2 laser. The infrared spectroscopy of CO_2 will first be introduced to provide the necessary background. The mode-temperature model and the calculation of gain coefficients in CO_2 will next be discussed as these topics form the basis of this thesis. Finally, a brief description will be given of the lasers used in this work -- the regular, sequence and 4.3 μm CO_2 lasers.

2.2 Infrared Spectrum of CO_2†

The CO_2 molecule is a linear symmetric triatomic molecule. To a good approximation, the total wavefunction Ψ is simply a product of the electronic, vibrational and rotational wavefunctions:

$$\Psi = \Psi_e \Psi_v \Psi_r \tag{2-1}$$

and the total energy is a sum of the three types of energies. As the CO_2 lasing states involve vib-rotational transitions in the ground

* Much of the material in this chapter was first presented by R.K. Brimacombe [16].

† The main reference for this section is Herzberg [17].

electronic state, only the vibrational and rotational energy levels will be discussed here.

The CO_2 molecule has 4 vibrational degrees of freedom. As shown in Fig. 2-1, these normal vibrations are the symmetric stretch (ν_1) mode, the doubly degenerate bending (ν_2) mode (vibrating in and out of the plane of the paper) and the asymmetric stretch (ν_3) mode. Each vibrational energy level is denoted by ($ij^{\ell}k$) where i, j and k are the number of quanta in the ν_1, ν_2 and ν_3 modes respectively, and ℓ is the vibrational angular momentum of the bending mode about the symmetry axis. The ℓ values are given by:

$$\ell = j,\ j-2,\ j-4,\ \ldots,\ 1 \text{ or } 0 \qquad (2\text{-}2)$$

depending on whether j is odd or even. The total degeneracy of the ν_2 mode is equal to j+1. Anharmonicity removes some of this degeneracy by splitting the different ℓ levels belonging to the same j. The remaining double degeneracy of each nonzero ℓ level is removed by ℓ-type doubling (See p. 9). In the simple harmonic oscillator (SHO) approximation, the total vibrational energy E_{vib} is given by:

$$E_{vib} = h\nu_1(i+1/2) + h\nu_2(j+1) + h\nu_3(k+1/2) \qquad (2\text{-}3)$$

where the fundamental frequencies of the vibrational modes are $\nu_1 = 1388\ cm^{-1}$, $\nu_2 = 667\ cm^{-1}$ and $\nu_3 = 2349\ cm^{-1}$. Fig. 2-2 shows some of the vibrational energy levels relevant to this thesis.

There are two important effects which perturb the CO_2 energy level diagram. Anharmonicity of the vibrations causes the energy of

FIGURE 2-1

The normal vibrational modes of the CO_2 molecule.

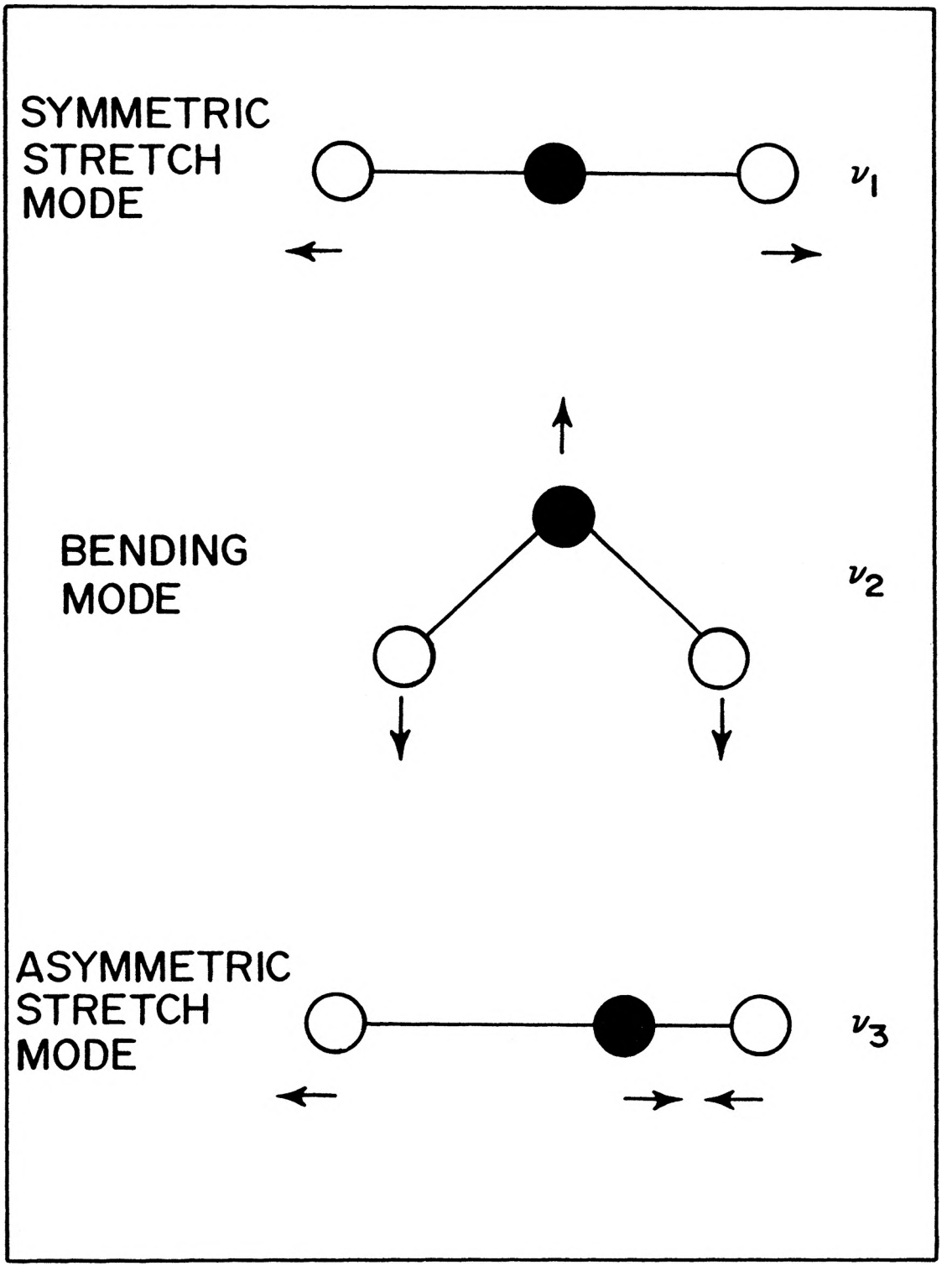
SYMMETRIC
STRETCH
MODE
ν_1
BENDING
MODE
ν_2
ASYMMETRIC
STRETCH
MODE
ν_3

FIGURE 2-2

Vibrational energy level diagram of CO_2 illustrating the main lasing transitions discussed in this work.

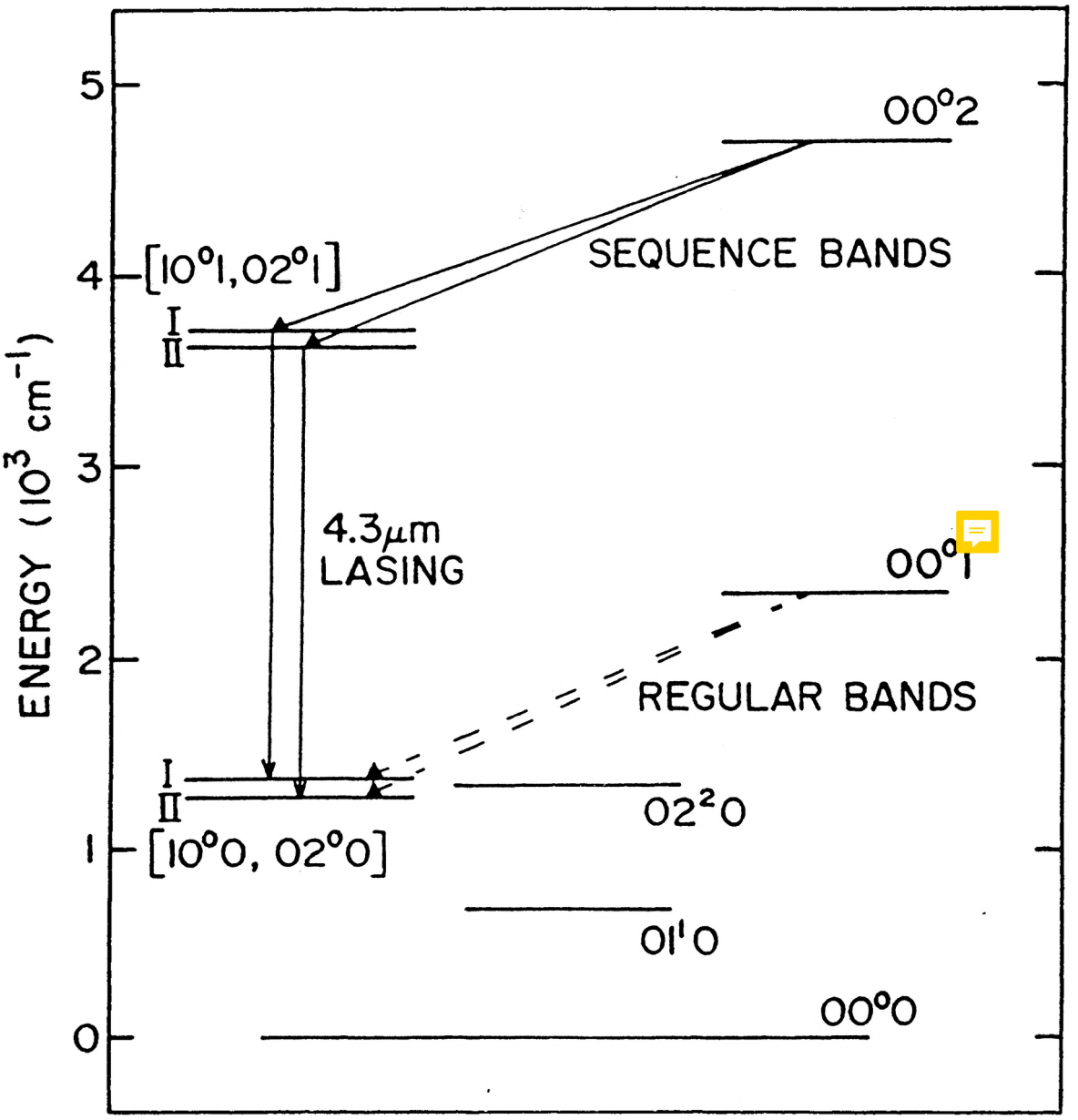
ENERGY (10^3 cm^{-1})
5
4
3
2
1
0
00^02
SEQUENCE BANDS
$[10^01, 02^01]$
I
II
4.3μm
LASING
00^01
REGULAR BANDS
I
II
02^20
$[10^00, 02^00]$
01^10
00^00

higher levels to be lower than that calculated by the SHO approximation. In the ν_3 mode, this causes the band centers of successive ν_3 transitions to decrease by ~ 25 cm^{-1} as k increases. Another perturbation of the molecular vibrations is caused by accidental degeneracy or Fermi resonance. Neglecting intermode interactions, the 10°0 and the 02°0 levels in CO_2 have almost the same calculated energy, 1337 cm^{-1} and 1334 cm^{-1} repectively. This close resonance causes a mixing of the eigenfunctions yielding true energy levels that are somewhat further apart, 1388 and 1285 cm^{-1} respectively. This phenomenon also takes place between members of higher-lying Fermi dyads (eg. [10°1-02°1], etc.), but it involves levels of the same species only (See discussion of species to follow). Due to the mixing of the eigenfunctions, the 10°0 and 02°0 levels should strictly be labeled as $[10°0,02°0]_I$ and $[10°0,02°0]_{II}$ respectively. (Only the shorter notation will be used in this work).

The symmetry properties of the vibrational levels are important in studying the normal vibrations of CO_2. The designation of the symmetry types or species of the normal vibrations is similar to that used for electronic states of homonuclear diatomic molecules. Each vibrational state is denoted by the species Σ, Π, Δ, Φ, ... corresponding to ℓ = 0, 1, 2, 3, ... respectively. In linear molecules, normal vibrations that are symmetric or antisymmetric with respect to a center of symmetry are denoted by the subscript g (gerade) or u (ungerade) respectively according to the following rule:

$$\begin{matrix}\text{Inversion}\\ \text{Symmetry}\end{matrix} = \begin{cases} g, \text{ if } (j+k) \text{ is even} \\ u, \text{ if } (j+k) \text{ is odd} \end{cases} \tag{2-4}$$

The superscript indicates the parity of the electronic eigenfunction and is always positive for the ground electronic state of CO_2. The species of the $00^{\circ}0$, $10^{\circ}0$, $01^{1}0$ and $00^{\circ}1$ levels are Σ_g^+, Σ_g^+, Π_u and Σ_u^+ respectively.

The rotational energies E_{rot} are superimposed on the vibrational energy levels and are given by:

$$E_{rot} = B_v J(J+1) - D_v J^2 (J+1)^2 + \ldots \tag{2-5}$$

where B_v is the rotational constant, D_v is the centrifugal constant and J is the rotational quantum number. The dependence of B_v on the particular vibrational level is due to the interaction of vibration and rotation. It is inversely proportional to the moment of inertia and therefore decreases with increasing vibrational energy. The higher order terms are small in comparison to the first term and are usually ignored (In CO_2, $B_v \sim 0.39$ cm^{-1}, $D_v \sim 10^{-7}$ cm^{-1}). The minimum value of J is equal to ℓ . The double degeneracy associated with each $\ell \neq 0$ state (Π, Δ, Φ, ...) is removed by rotation of the molecule and is called ℓ-type doubling. The result is that each J level is split into two components whose separation increases with increasing J. The two sets of levels that result are designated e and f (formerly c and d) since each set has a slightly different rotational constant B. For symmetric vibrational species (g), the even J levels are denoted e, the odd f. The reverse is true is true for (u) vibrational species.

The symmetry properties of the rotational levels are important in applying the selection rules to determine the allowed transitions. Each rotational level is labelled either positive (+) or negative (-) depending on the parity of the *total* eigenfunction. Therefore for the Σ^+ species, the parity of the rotational levels is equal to $(-1)^J$. In Π, Δ, ... levels, each J level has a positive and negative level of slightly different energy due to ℓ-type doubling (See Fig. 2-3). For linear molecules with a center of symmetry, the rotational levels are also labelled symmetric (s) or antisymmetric (a) with respect to a simultaneous exchange of all pairs of identical nuclei. In CO_2, the two ^{16}O nuclei are bosons. This requires the total eigenfunction to be exchange symmetric and all the antisymmetric rotational levels be absent. That is, the allowed J levels for $\ell = 0$ species are those that maintain $(-1)^{j+k+J} = 1$. This results in J levels that are either all odd or all even. For $\ell \neq 0$ states, the symmetry rule still applies, but all J levels are present due to ℓ-type doubling. (Note that for CO_2 with two different oxygen isotopes, both (s) and (a) rotational levels are present).

The selection rules governing the infrared spectrum of CO_2 are:*

$$\Delta\ell = 0, \pm 1; \quad \Sigma^+ \leftarrow/\rightarrow \Sigma^-, \; g \leftarrow/\rightarrow g, \; u \leftarrow/\rightarrow u \qquad (2\text{-}6)$$

for vibrational transitions and

---

* $\Delta\ell = \ell_{upper} - \ell_{lower}$; similarly for ΔJ.

FIGURE 2-3

Symmetry properties of the rotational levels in various species of CO_2 (from Herzberg [17]).

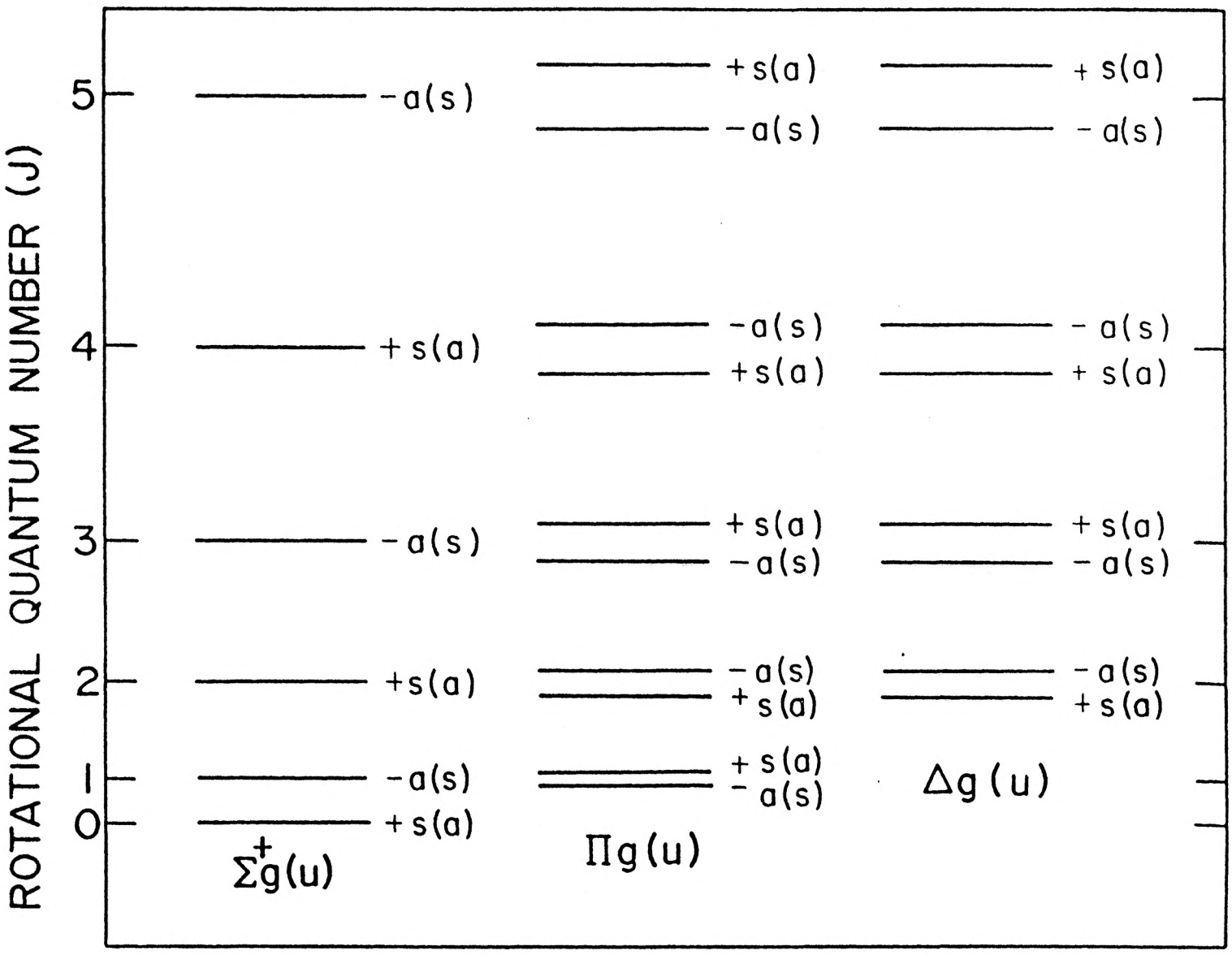
ROTATIONAL QUANTUM NUMBER (J)
5
4
3
2
1
0
-a(s)
+s(a)
-a(s)
+s(a)
-a(s)
+s(a)
$\Sigma_g^+(u)$
+s(a)
-a(s)
+s(a)
-a(s)
+s(a)
-a(s)
+s(a)
-a(s)
+s(a)
-a(s)
$\Pi g(u)$
+s(a)
-a(s)
+s(a)
-a(s)
+s(a)
-a(s)
+s(a)
-a(s)
$\Delta g(u)$

$$\Delta J = 0, \pm 1; \quad (J=0 \leftarrow/\rightarrow J=0), \; + \longleftrightarrow -, \; s \leftarrow/\rightarrow a \qquad (2\text{-}7)$$
$$\Delta J \neq 0 \quad \text{for } \Sigma\text{-}\Sigma \text{ transitions}$$

for rotational transitions.

All the infrared bands of CO_2 contain lines in the P branch ($\Delta J = -1$) and R branch ($\Delta J = 1$). The Q branch ($\Delta J = 0$) only exists when either one or both vibrational levels have $\ell \neq 0$. For parallel bands ($\Delta\ell = 0$), the Q branch is weak (absent for Σ-Σ transitions).* It is only in perpendicular bands ($\Delta\ell = \pm 1$) that the Q branch dominates. The convention is to use the lower rotational quantum number J to label the various branches (eg. P(J) or R(J)). Fig. 2-4 illustrates in detail some of the lasing transitions in CO_2.

It is fortunate that even under lasing conditions, the population distribution of CO_2 over its various energy levels is still relatively simple. The key to this simplification lies in the molecular relaxation processes of CO_2 as will be explained in the next section.

2.3 Collisional Relaxation Processes

The lifetimes of the laser levels in the CO_2 laser are governed by collisional mechanisms. Other processes such as spontaneous emission and wall diffusion become important only at low pressures. Table 2-1 lists the major collisional relaxation rates in CO_2 as well as typical values for the CO_2 mixtures used in this thesis. There are three types of molecular collision processes: rotation-to-translation (R-T)

---

* Only parallel bands are studied in this work.

FIGURE 2-4

Vibrational energy level diagram detailing some of the vib-rotational transitions in the regular, sequence and 4.3 μm bands of CO_2. The energy spacing between the rotational levels is exaggerated.

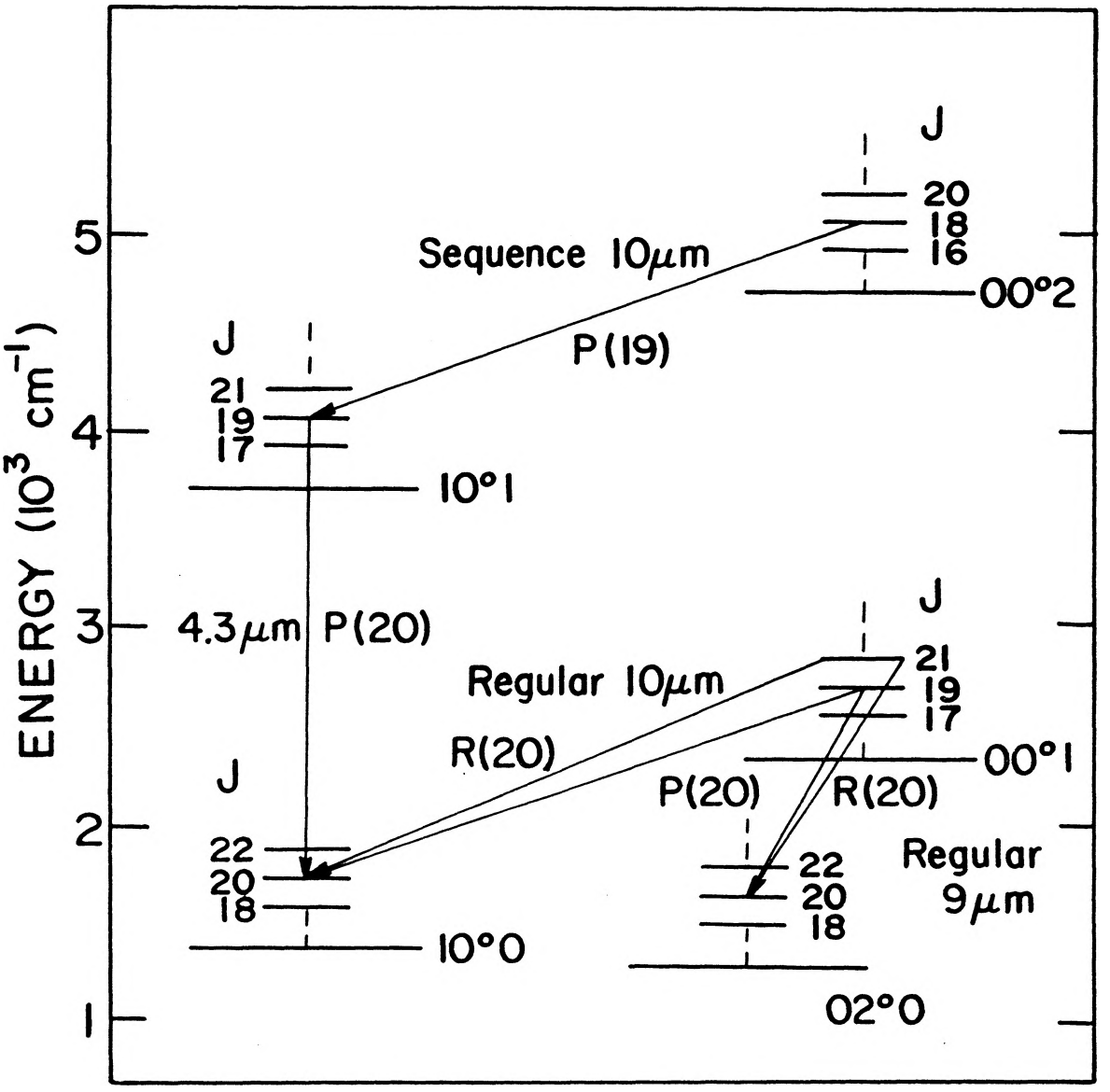
ENERGY (10^3 cm^{-1})
5
4
3
2
1
J
20
18
16
00°2
Sequence 10μm
P(19)
J
21
19
17
10°1
4.3μm P(20)
J
21
19
17
Regular 10μm
R(20)
00°1
J
22
20
18
10°0
P(20)
R(20)
22
20
18
Regular
9μm
02°0

TABLE 2-1

Summary of various collisional relaxation rates and their temperature dependences in CO_2 (adapted from Ref. [16]). Collisional lifetimes are calculated for a typical mixture employed in this work.

Relaxation Rate* ($s^{-1}Torr^{-1}$)	Reference	2% CO_2 : 98% He 1000 Torr, T=300 K
$k_R(CO_2) = 1.3x10^7$	[18]	
$k_R(N_2) = 1.2x10^7$	[18]	$\tau_R = 0.2$ ns
$k_R(He) = 0.6x10^7$	[18]	
$k_{\nu_3}(CO_2) = 13.7x10^6 (300/T)^{1.258}$	[21]	$\tau_{\nu_3} = 3.7$ ns
$k_{101}(CO_2) = 4.2x10^6(295/T)^{1.117}$	[20,21,24]	$\tau_{101} = 9.1$ ns
$k_{101}(N_2,He) = k_{100}(N_2,He)$	[16]	
$k_{100}(CO_2) = 4.3x10^5$	[6,26]	$\tau_{100} = 28$ ns
$k_{100}(N_2,He) = 2.5x10^4(T/280)^{1.5}$	[6,26]	
$k_{VT}(CO_2) = 187exp[3.77x10^{-3}(T-300)]$	[27]	
$k_{VT}(N_2) = 115exp[5.98x10^{-3}(T-300)]$	[28]	$\tau_{VT} = 267$ ns
$k_{VT}(He) = 3825exp[7.14x10^{-3}(T-300)]$	[29]	
$k_{N_2}(CO_2) = 8.6x10^7 T^{-1.5}$	[25]	$\tau_{N_2} = 3\ \mu s$ (in 2% CO_2:2% N_2:96% He)
$k_3(CO_2) = 94 + 0.818T,\ 250K < T < 400K$	[27]	
$k_3(N_2) = 10^{(4.44-16T^{-1/3})}$	[25]	$\tau_3 = 11.6\ \mu s$
$k_3(He) = 21.4 + 0.2T$	[29]	

* Valid for temperatures from approximately 300 K to 500 K.

relaxation, vibration-to-vibration (V-V) transfer and vibration-to-translation (V-T) relaxation.

The fastest process is the R-T relaxation rate k_R. This rate is comparable to the gas kinetic collision rate and generally ensures the rotational levels within each vibrational manifold are in thermal equilibrium with the background gas temperature T. The measured rate constants are $k_R(CO_2) = 1.3\times10^7\ s^{-1}Torr^{-1}$, $k_R(N_2) = 1.2\times10^7\ s^{-1}Torr^{-1}$ and $k_R(He) = 0.6\times10^7\ s^{-1}Torr^{-1}$ [18]. These values have been confirmed in other experiments [19,20] and are independent of temperature.

The fastest V-V process is the ν_3 intra-mode relaxation rate k_{ν_3} which occurs through processes such as:

$$2\ CO_2(00^01) \xrightarrow{k_{\nu_3}} CO_2\ (00^02) + CO_2(00^00) \qquad (2\text{-}8)$$

A value of $k_{\nu_3} = 13.7\times10^6\ s^{-1}\ Torr^{-1}$ at 300 K has been calculated for this process [21]. Similar fast intramode relaxation processes occur in the ν_1 and ν_2 modes [4].

There are many processes that couple energy into the 00^01 level and help redistribute energy within the ν_3 mode of CO_2 [22-24]. Some of these are outlined below.

The 10^01 level is the upper laser level of the 4.3 μm CO_2 laser and also the upper level of the absorbing transition in optically-pumped CO_2. This level relaxes through the process:*

$$CO_2(10^01) + CO_2(00^00) \xrightarrow{k_{101}} CO_2\ (10^00) + CO_2\ (00^01) \qquad (2\text{-}9)$$

* A similar mechanism exists for the 02^01 level.

with a measured rate constant of $k_{101}(CO_2) = 4.2\times10^6\ s^{-1}Torr^{-1}$ at 295 K [24]. The rates $k_{101}(N_2,He)$ are assumed to be equal to $k_{100}(N_2,He)$ [16]. This fast relaxation process is detrimental to 4.3 μm lasing but at the same time is responsible for efficiently coupling excess population from the 10°1 level into the ν_3 mode.

Another process which couples energy into the ν_3 mode involves the energy transfer of vibrationally-excited N_2 to the 00°1 level of CO_2; i.e.,

$$CO_2\ (00^\circ0) + N_2(1) \xrightarrow{k_{N_2}} CO_2\ (00^\circ1) + N_2(0) \qquad (2\text{-}10)$$

Due to the close resonance of the $N_2(v=1)$ level with 00°1 and the forbidden radiative decay of the v=1 state to the ground state, this reaction proceeds mainly in the forward direction and is highly efficient in exciting CO_2. The process in (2-10) has a measured rate constant k_{N_2} of $1.66\times10^4\ s^{-1}Torr^{-1}$ at 300 K [25].

The levels 10°0 and 02°0 form the lower laser levels of the regular and 4.3 μm CO_2 laser. The 10°0 level decays relatively quickly to the many vibrational levels nearby:

$$CO_2\ (10^\circ0) + M \longrightarrow CO_2\ (02^20) + M \qquad (2\text{-}11)$$

$$CO_2\ (10^\circ0) + M \longrightarrow CO_2\ (02^\circ0) + M \qquad (2\text{-}12)$$

$$CO_2\ (10^\circ0) + CO_2\ (00^\circ0) \longrightarrow 2\ CO_2\ (01^10) \qquad (2\text{-}13)$$

where M is the collision partner. The 02°0 level decays in a similar fashion. The measured rate constants for all three processes are

$k_{100}(CO_2) = 4.3\text{x}10^5\ s^{-1}Torr^{-1}$, and $k_{100}(N_2) = k_{100}(He) = 2.5\text{x}10^4\ s^{-1}Torr^{-1}$ [26]. Much uncertainty remains in the values of these constants and their temperature dependences. As a compromise, $k_{100}(CO_2)$ is assumed to be independent of temperature, and $k_{100}(He)$ and $k_{100}(N_2)$ assumed to vary as $T^{1.5}$ [6]. The values of these constants as well as their temperature dependences have been shown to give good agreement in 4.3 μm CO_2 laser modeling [6].

Although processes (2-11) to (2-13) occur fairly quickly, the relaxation of the lower laser levels are ultimately governed by the decay of the ν_1 and ν_2 mode through the slower V-T process:

$$CO_2\ (01^10)\ +\ M \xrightarrow{k_{VT}} CO_2\ (00^00)\ +\ M \qquad (2\text{-}14)$$

The rate constants as well as their temperature dependence are well known for this process. They are $k_{VT}(CO_2) = 187\ s^{-1}Torr^{-1}$ [27], $k_{VT}(N_2) = 115\ s^{-1}Torr^{-1}$ [28] and $k_{VT}(He) = 3825\ s^{-1}Torr^{-1}$ at 300 K [29]. Due to the high efficiency with which He depopulates the 01^10 level and hence the lower laser levels, it is a major constitutent of CO_2 laser mixtures.

The intermode decay of the ν_3 mode occurs primarily through the 00^01 level. The 00^01 decay rate is slow compared to that of the lower laser levels. This slow relaxation rate is partly responsible for the high efficiency and output power of regular band CO_2 lasers. The energy in the ν_3 mode decays slowly into the other two modes through the V-V process:

$$CO_2\ (00^01)\ +\ M \xrightarrow{k_3} CO_2\ (ij^{\ell}0)\ +\ M \qquad (2\text{-}15)$$

The rate constants for this process are accurately known as a function of temperature; they are $k_3(CO_2) = 339\ s^{-1}Torr^{-1}$ [27], $k_3(N_2) = 112\ s^{-1}Torr^{-1}$ [25] and $k_3(He) = 81\ s^{-1}Torr^{-1}$ at 300 K [29].

The highly differential relaxation processes in CO_2 discussed in this section can be used to create a simple model of CO_2 laser dynamics. A detailed description of this highly successful model will be given in the next section.

2.4 Mode-Temperature Model

The basis of the mode-temperature model is that the intramode relaxation rate in CO_2 is much faster than the intermode decay and the V-T transfer rate. Therefore an equilibrium is established amongst the various levels in each vibrational mode. Under low excitation of a mode, the population distribution in low-lying levels can be accurately described by a Boltzmann distribution characterized by a single vibrational temperature [3,4]. This temperature is usually different from the other mode temperatures and the background temperature of the gas. Under high excitation, a Treanor distribution [14,15] characterized by a vibrational temperature and a translational temperature must be used instead. Since they were first proposed, both the Boltzmann and Treanor mode-temperature models have been verified in many experiments [2,7].

In the Boltzmann mode-temperature model, the ν_1, ν_2 and ν_3 modes are each characterized by their respective temperatures T_1, T_2 and T_3. Due to the strong coupling between the ν_1 and ν_2 modes, T_1 is usually

equal to T_2 [2]. The power of the mode-temperature model lies in its ability to calculate the population of any level once all the mode temperatures are known. The population of a vibrational level $N_{ij\ell_k}$ is given by:

$$N_{ij\ell_k} = \frac{N_{CO_2} d_j (x_1)^i (x_2)^j (x_3)^k}{Q_v} \tag{2-16}$$

where N_{CO_2} is the number density of CO_2 molecules

$d_j = j+1$, (the degeneracy of the ν_2 mode)

$x_n = \exp(-h\nu_n/k_BT_n)$

$Q_v = [(1-x_1)(1-x_2)^2(1-x_3)]^{-1}$, (the vibrational partition function)

Due to their rapid relaxation rate, all the rotational levels are in thermal equilibrium with the background gas and have the same temperature, T. The population of a vib-rotational level $N_{ij\ell_{k;J}}$ is given by:

$$N_{ij\ell_{k;J}} = N_{ij\ell_k} K(J) \tag{2-17}$$

where $K(J) = \frac{g_J}{Q_R} \exp[-BJ(J+1)/k_BT]$

$g_J = 2J+1$

Q_R is the rotational partition function

$$= \begin{cases} \frac{k_BT}{2Bhc}, & \text{alternate J levels missing} \\ \frac{k_BT}{Bhc}, & \text{all J levels present} \end{cases}$$

In CO_2 at room temperature, the peak of the rotational distribution is at $J \simeq 18$.

If the anharmonicity of the vibrations is included in the calculations, then the Boltzmann factors in (2-16) must be replaced by a Treanor distribution [14,15]. Fortunately, only the ν_3 mode is affected in the optical pumping scheme used in this work. In a Treanor distribution, the population in the 00°k level is given by:

$$N_k = N_0 \exp[-hc(kG_1/T_3^* - \Delta G_k/T)/k_B] \tag{2-18}$$

where N_0 is the population in the ground state,

G_1 is the energy spacing between the 00°1 level and the ground state,

ΔG_k is the difference between the energy level calculated by the SHO approximation and the actual energy of the level,

T_3^* is the Treanor vibrational temperature,

T is the translational temperature

and the other symbols have their usual meanings. The population of a Treanor vibrational level $N^*_{ij\ell_k}$ then becomes:

$$N^*_{ij\ell_k} = \frac{N_{CO_2}\, d_j (x_1)^i\, (x_2)^j N_k^*}{Q_v^*} \tag{2-19}$$

where $N_k^* = N_k/N_0$

and $Q_v^* = (\sum_{k=0}^{9} N_k^*) / [(1-x_1)(1-x_2)^2]$ †

The Treanor distribution becomes important in the calculation of high-lying ν_3 mode populations when the Boltzmann temperature T_3 exceeds ~ 2000 K [2].

Once the population distribution in the ν_3 mode is known, it is straightforward to calculate the energy stored in the mode. In the Boltzmann case, the ν_3 mode energy E_3 is given by:

$$E_3 = N_{CO_2} h\nu_3 \, x_3 / (1-x_3) \tag{2-20}$$

In a Treanor distribution, the mode energy E_3^* is approximated by:

$$E_3^* = N_{CO_2} (\sum_{k=1}^{9} E_k N_k^*) / \sum_{k=0}^{9} N_k^* \tag{2-21}$$

For the same amount of energy in the ν_3 mode, more population is placed and more energy stored in the upper levels of the ν_3 mode in a Treanor distribution than in a Boltzmann distribution.

The three Boltzmann vibrational temperatures in CO_2 are easily determined experimentally by the measurement of a few gain coefficients [1]. The rotational temperature (and the translational temperature) T can be determined by a least squares fit of the rotational gain

† The summation is truncated at the 00°9 level as much uncertainty remains in the distribution of the ν_3 mode population above this level. The validity of this truncation will be demonstrated in Chapter 3.

distribution [30,31]. In the next section, the method of calculating gain coefficients in CO_2 will be detailed.

2.5 Gain Coefficient

In order to fully understand any laser system, one must be able to accurately predict the gain coefficient over a wide range of conditions. The spectroscopy of CO_2 has been extensively studied over the years and an accurate expression for the gain coefficient in the low excitation limit can be given. This expression has been verified with experiment [1] and will be slightly modified for the Treanor distribution in this thesis.

For the vib-rotational levels in a gas, the gain coefficient $\gamma(\nu)$ between the upper (u) and lower (l) level is written as:

$$\gamma(\nu) = [\lambda_0^2/(8\pi)]\ A_{ul}\ g(\nu)\ [N_u K_u - (g_u/g_l) N_l K_l] \qquad (2\text{-}22)$$

where λ_0 = wavelength center of the transition

A_{ul} = spontaneous transition rate

$g(\nu)$ = normalized lineshape function

$N_{u(l)}$ = number density of the vibrational population of the upper (lower) level (See previous Section)

$K_{u(l)}$ = fraction of the vibrational population in the $J_{u(l)}$ level (See previous section)

and $g_{u(l)} = 2J_{u(l)} + 1$

Each of these factors has been thoroughly investigated [16] and only a summary of the results will be given.

The frequencies of the CO_2 laser lines are very well known. Explicit expressions exist for calculating P, Q and R branch transitions in various bands of CO_2 [32-35].

The spontaneous transition rate A_{ul} is given by [36]:

$$A_{ul} = \frac{64\pi^4 |R_{ul}|^2 S_J F_J}{3h\lambda_o^3 g_u} \tag{2-23}$$

where $|R_{ul}|$ = vibrational contribution to the transition dipole moment

S_J = rotational contribution to the moment

F_J = vibration-rotation interaction factor

$J = J_{lower}$

and $g_u = 2J_u + 1$

The constant S_J is calculated from the expressions given in Table 2-2. The values of $|R_{ul}|$ and F_J are obtained by fitting absorption data to the expression for gain at a fixed linewidth [1,16]. Table 2-3 gives these values for various bands in CO_2 . The ratios $|R_{ul}|^2/|R_{00°1}|^2$ have been measured in various bands and are important in the measurement of mode temperatures. For transitions which have not been measured, F_J is set to unity and the SHO approximation is used to obtain $|R_{ul}|$ (eg. $|R_{00°2-00°1}|^2 = 2|R_{00°1-00°0}|^2$).

The lineshape function $g(\nu)$ is, in general, a convolution of Doppler and collisional broadening, (the Voight profile), and is given by:

TABLE 2-2

Calculation of S_J for P, Q and R branch transitions in parallel bands of CO_2 (derived from [16]). J is the rotational quantum number of the lower level.

Branch	S_J	
	$\ell = 0$	$\ell \neq 0$
P	J	$\frac{2(J^2-\ell^2)}{J}$
Q	0	$\frac{3\ell^2(2J+1)}{J(J+1)}$
R	J+1	$\frac{2[(J+1)^2-\ell^2]}{J+1}$

TABLE 2-3

Measured transition moment factors F_J and $|R_{ul}|$ in CO_2 (adapted from [16]).

Band	F_J	$\lvert R_{ul}\rvert$ (Debye)	$\frac{\lvert R_{ul}\rvert^2}{\lvert R_{00^01}\rvert^2}$
$00^01 - 10^00$	$1 - 1.8\times10^{-3}m + 3.7\times10^{-5}m^2$	0.0371	
$00^01 - 02^00$	$1 - 2.4\times10^{-4}m + 4.1\times10^{-5}m^2$	0.0339	
$00^02 - 10^01$	same as $(00^01 - 10^00)$		2.1
$00^02 - 02^01$	same as $(00^01 - 02^00)$		1.89
$01^11 - 11^10$	same as $(00^01 - 10^00)$		0.54
$10^01 - 10^00$	1	0.3116	
$00^01 - 00^00$	1	0.3237	

$$g(\nu) = \frac{1}{\pi^{3/2}\Delta\nu_c}\int_{-\infty}^{\infty}\frac{y^2\exp(-t^2)}{y^2+(x-t)^2}\,dt \qquad (2\text{-}24)$$

where $\Delta\nu_c$ = collisional linewidth (HWHM)

$$y = \sqrt{\ln 2}\,\frac{\Delta\nu_c}{\Delta\nu_D}$$

$$x = \sqrt{\ln 2}\,\frac{\nu-\nu_o}{\Delta\nu_D}$$

and $\Delta\nu_D$ is the Doppler-broadened linewidth (HWHM).

This integral can be evaluated numerically for any x and y as shown in [37]. At line center, $\nu = \nu_0$, and the lineshape function becomes

$$g(\nu_o) = \frac{y\exp(y^2)}{\sqrt{\pi}\,\Delta\nu_c}\,\mathrm{erf}(y) \qquad (2\text{-}25)$$

where erfc(y) is the complementary error function. If collisional broadening dominates (ie. y > 3), then $g(\nu)$ simplifies to the normalized Lorentzian lineshape function:

$$g(\nu) = \frac{1}{\pi\Delta\nu_c}\cdot\frac{1}{1+[(\nu-\nu_o)/\Delta\nu_c]^2} \qquad (2\text{-}26)$$

The Doppler linewidth $\Delta\nu_D$(HWHM) is given by:

$$\Delta\nu_D = \frac{\nu_o}{c}\sqrt{\frac{2k_BT\ln 2}{M}} \qquad (2\text{-}27)$$

where M is the mass of the CO_2 molecule. This has a value of ~27 MHz for 10 μm transitions and ~65 MHz for 4.3 μm transitions.

The collision broadened linewidth $\Delta\nu_c$ (HWHM) has been accurately measured and is given (in cm^{-1}) by [38]:

$$\Delta\nu_c = \frac{P}{760}\left(f_{CO_2}\alpha_{CO_2} + f_{N_2}\alpha_{N_2} + f_{He}\alpha_{He}\right) \begin{cases} \left(\frac{T}{300}\right)^{0.42}, & \text{constant number density} \\ \left(\frac{300}{T}\right)^{0.58}, & \text{constant pressure} \end{cases} \tag{2-28}$$

where $\alpha_{CO_2} = 0.1149 - 9.2\text{x}10^{-4}\,|m|$

$\alpha_{N_2} = 0.0794 - 4.3\text{x}10^{-4}\,|m|$

$\alpha_{He} = 0.0598 - 2.8\text{x}10^{-5}\,|m|$

and $m = \begin{cases} -J_\ell, & \text{P-Branch} \\ J_\ell + 1, & \text{R-Branch} \end{cases}$

For typical CO_2 laser mixtures, $\Delta\nu_c$ is ~2.5 MHz/torr. Theoretical and experimental results show that collisional linewidths differ very little between bands [39-42], hence the linewidth expression is assumed to be band-independent in this work. In CO_2, there are often many transitions whose lineshape functions overlap one another. These "overlapping contributions" must be summed in order to accurately calculate gain at a particular frequency.

All the factors appearing in the gain expression (2-22) have now been fully described and the gain coefficient can be easily calculated given the mixture, pressure and the three temperatures T_1, T_3 and T. A computer model based on this expression has predicted gain to within ±10% of experimental values over a wide range of conditions [1,16].

This model can therefore be confidently applied to the optical pumping of CO_2 at 4.3 μm.

The preceding sections have provided the foundation for understanding CO_2 laser theory. In the following sections, this background material will be used to explain the gain dynamics of an optically-pumped CO_2 system as well as describe the pump and probe sources used in these experiments.

2.6 New Wavelength CO_2 Lasers

The inversion mechanisms and output characteristics of the regular, sequence and 4.3 μm CO_2 lasers are discussed in this section.

In a conventional CO_2 laser, gain is created on the regular bands (00°1-10°0 or 00°1-02°0) by the combined processes of electron excitation and molecular relaxation. A CO_2:N_2:He gas mixture is excited in a pulsed electrical discharge. All the low-lying levels in CO_2 and the first vibrationally-excited state of N_2 are populated by electron excitation. The population in the ν_1 and ν_2 modes decay rapidly compared to those in the ν_3 mode. As a result, after several V-T times, population inversion and gain will exist in the 00°1-02°0 (10.4 μm) and 00°1-02°0 (9.4 μm) bands. For a typical gas mixture of 20% CO_2 : 20% N_2 : 60% He at atmospheric pressure in a one metre long discharge with a 10 cm^2 aperture, output pulse energies of > 10 J and peak powers of 40 MW can be obtained [16]. By varying the mixture and discharge conditions, more than 80 lines in the P and R branches of both the 9 and 10 μm bands can be made to lase.

The operation of a sequence CO_2 laser takes advantage of the fact that in a discharge, gain exists not only on the (00°1-10°0) band but also on the higher-lying (00°n-10°(n-1)) bands as well.* For the experiments in this work, only the (00°2-10°1) sequence band laser was used. Lasing is achieved on the sequence bands by suppressing the (higher) gain on the regular bands with a hot CO_2 gas cell [43]. Due to the anharmonicity of the vibrations, the sequence band frequencies are slightly different from those of the regular bands (The separation between a sequence line and the nearest regular line is often < 1 cm^{-1}). Sequence oscillation has been achieved in both cw and pulsed modes. With a 12% CO_2 : 20% N_2 : 68% He mixture at one atmosphere and a hot cell containing 450 Torr of CO_2 (T ~ 600 K), sequence pulse energies of > 2 J were obtained on 30 lines in the 00°2-10°1 and 00°2-02°1 sequence bands in a one metre long pulsed discharge [44].

The 4.3 μm CO_2 laser is a natural extension of the use of a sequence laser as an optical pump source. Its theory of operation is quite simple. Gain is produced on the regular and sequence bands of a CO_2 laser gas mixture in a pulsed electrical discharge. When the sequence gain reaches a peak, an externally-generated sequence laser pulse is directed into the discharge. This transfers much population from the 00°2 level to the 10°1 level thereby creating gain on the (10°1-10°0) band. In an appropriate cavity, lasing can then take place at ~ 4.3 μm. Due to high absorption at this wavelength in excited CO_2 laser gas mixtures, the 4.3 μm CO_2 laser is operated at relatively low

* Gain has been measured up to the n=4 band [7].

CO_2 content and pressures (~4% CO_2 and ~60 Torr). Since it was reported in 1979 by Znotins et al. [45], 4.3 μm laser pulse energies and powers have improved to 15 mJ and 100 kW respectively on the (10°1-10°0) P(26) transition [46]. A total of 28 lines in the (10°1-10°0) and (02°1-02°0) band have been observed to lase. Unfortunately, the short lifetime of the 10°1 level as compared to that of the 10°0 level precludes the possibility of cw laser oscillation at 4.3 μm. Nevertheless, the pulsed 4.3 μm CO_2 laser exists as a powerful tool for exploring the gain mechanisms of the CO_2 laser system.

2.7 Summary

This chapter has reviewed the main points of CO_2 laser theory which are necessary in understanding the physics of excited CO_2 media. The technique used for calculating gain coefficients in CO_2 has been confirmed in many experiments and provides a solid basis for studying optically-pumped CO_2. In the following chapters, the experimental technique and results of this investigation are presented.

Chapter 3

EXPERIMENTAL PROCEDURE

3.1 Introduction

The technique used in the present work to characterize optically-pumped CO_2 can be described as double resonance laser spectroscopy. A 4.3 μm CO_2 pump laser is used to excite the CO_2 gas while a cw 10 μm CO_2 probe laser measures the regular and sequence band gain. There are alternative pump sources available in the 4 μm region -- DF, HBr, and HCl lasers [47], some of which (HCl and HBr) have yielded pulse energies of 30 mJ [48] and higher [49]. The sequence-pumped 4.3 μm laser compares favourably with these other sources. It has the primary advantage of being entirely based on well-developed CO_2 laser technology thus ensuring reliability and ease of operation. For similar reasons, a conventional cw CO_2 laser was chosen as the probe source. Although a tunable diode laser would have yielded more information about the population distribution in the ν_3 mode, its high susceptibility to electromagnetic noise would have presented many additional difficulties.

The apparatus described in this chapter was used (with minor cell length changes) for gain measurements in both dilute and high-CO_2 content mixtures. The configuration used in attempting to create a Treanor laser in CO_2 will be discussed in the next chapter.

3.2 Experimental Apparatus

The apparatus used for determining the degree of excitation of the ν_3 mode essentially consists of the 4.3 μm CO_2 laser, a cw CO_2 probe laser and a waveguide cell. A schematic diagram is shown in Fig. 3-1.

The 4.3 μm CO_2 laser system consists of a TEA hybrid sequence laser and a 4.3 μm oscillator as shown in Fig. 3-2. The sequence laser comprises a Lumonics K-902-2 TEA discharge module with an active gain cross-section of 3.3 x 3.5 cm^2 (the brass electrode spacing is 3.3 cm) and a gain length of 44 cm. The intra-cavity hot cell is 60 cm in length and is filled with 450 Torr of CO_2 at a temperature of 550 K. The low pressure "hybrid" discharge has a 25 cm gain length and is operated with a flowing gas mixture (~ 200 ml/min NTP) of 5% CO_2 : 10% N_2 : 85% He at ~ 20 Torr. The low pressure section reduces the spectral linewidth of the sequence pump laser to more closely match the linewidth of the 4.3 μm oscillator. A PTR ML-304 original grating (135 lines/mm) and a 65% reflecting mirror (25 m radius of curvature) form the rest of the ~ 2.3 m-long cavity. In the main TEA discharge, a flowing gas mixture (~ 6 ℓ/min NTP) of 9% CO_2 : 14% N_2 : 77% He at ~ 780 Torr was excited with input energies of ~ 210 J/ℓ·atm. Output pulse energies of > 1 J and pulse widths of ~ 300 ns FWHM were obtained on the strongest sequence lines. The sequence output was allowed to expand over a 3.5 m distance in order to fill the aperture of the TE low pressure discharge. The 4.3 μm oscillator consists of two Lumonics K-902-2 modules with a total gain length of 88 cm. A dichroic flat (90% transmitting at 10 μm, 87% reflecting at 4.3 μm) forms the entrance aperture of the discharge

FIGURE 3-1

Schematic diagram of the apparatus used for T_3 measurements. The dichroic mirror transmits 90% at 10 μm and reflects 87% at 4.3 μm. The CO_2 cell near the detector absorbs any residual 4.3 μm radiation.

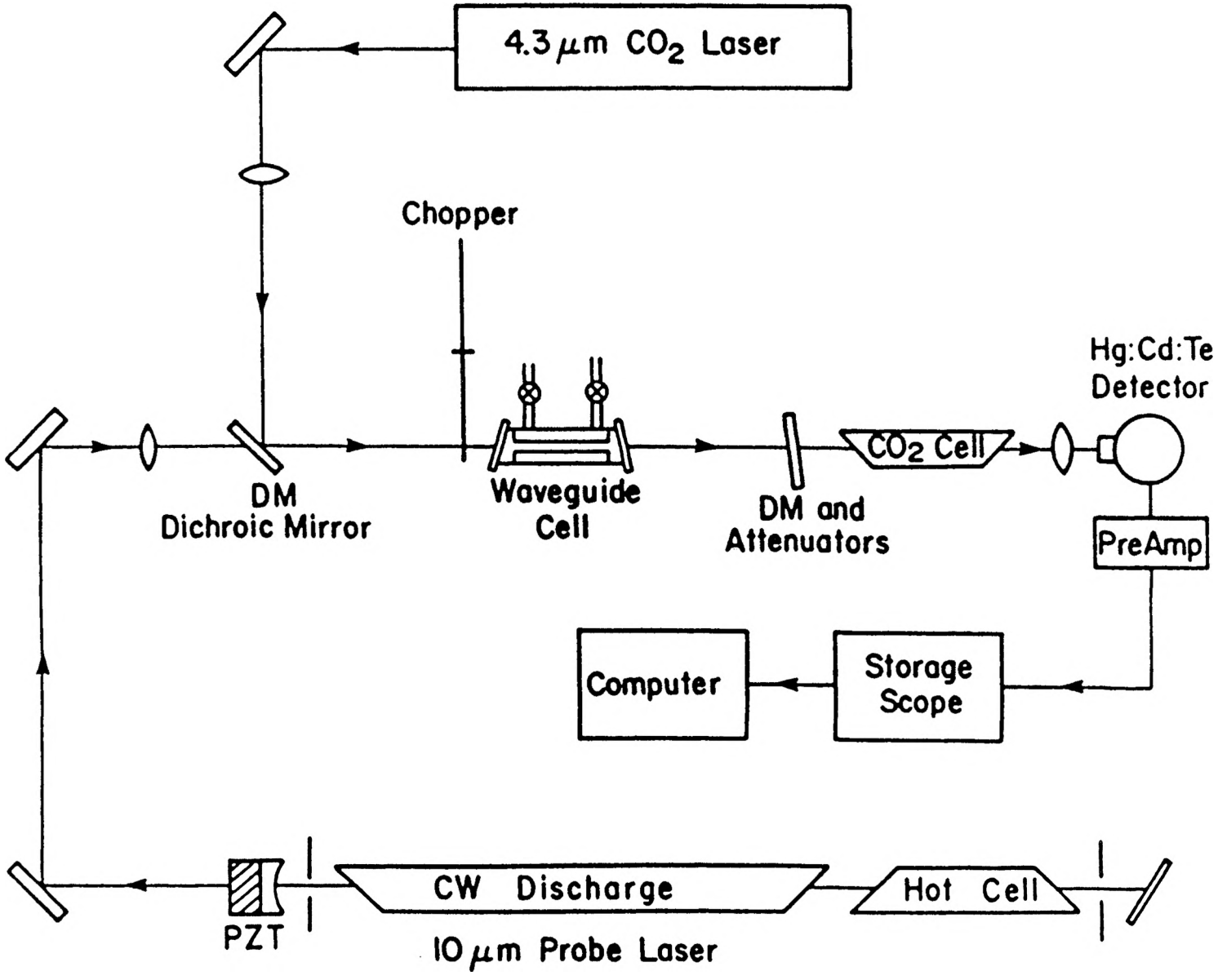
4.3 μm CO2 Laser
Chopper
Hg:Cd:Te
Detector
DM
Dichroic Mirror
Waveguide
Cell
DM and
Attenuators
CO2 Cell
PreAmp
Computer
Storage
Scope
PZT
CW Discharge
Hot Cell
10 μm Probe Laser

FIGURE 3-2

Schematic diagram of the 4.3 μm laser system. The LiF flat absorbs all of the sequence radiation and transmits ~ 90% of the 4.3 μm radiation. The dichroic mirror is similar to that used in Figure 3-1.

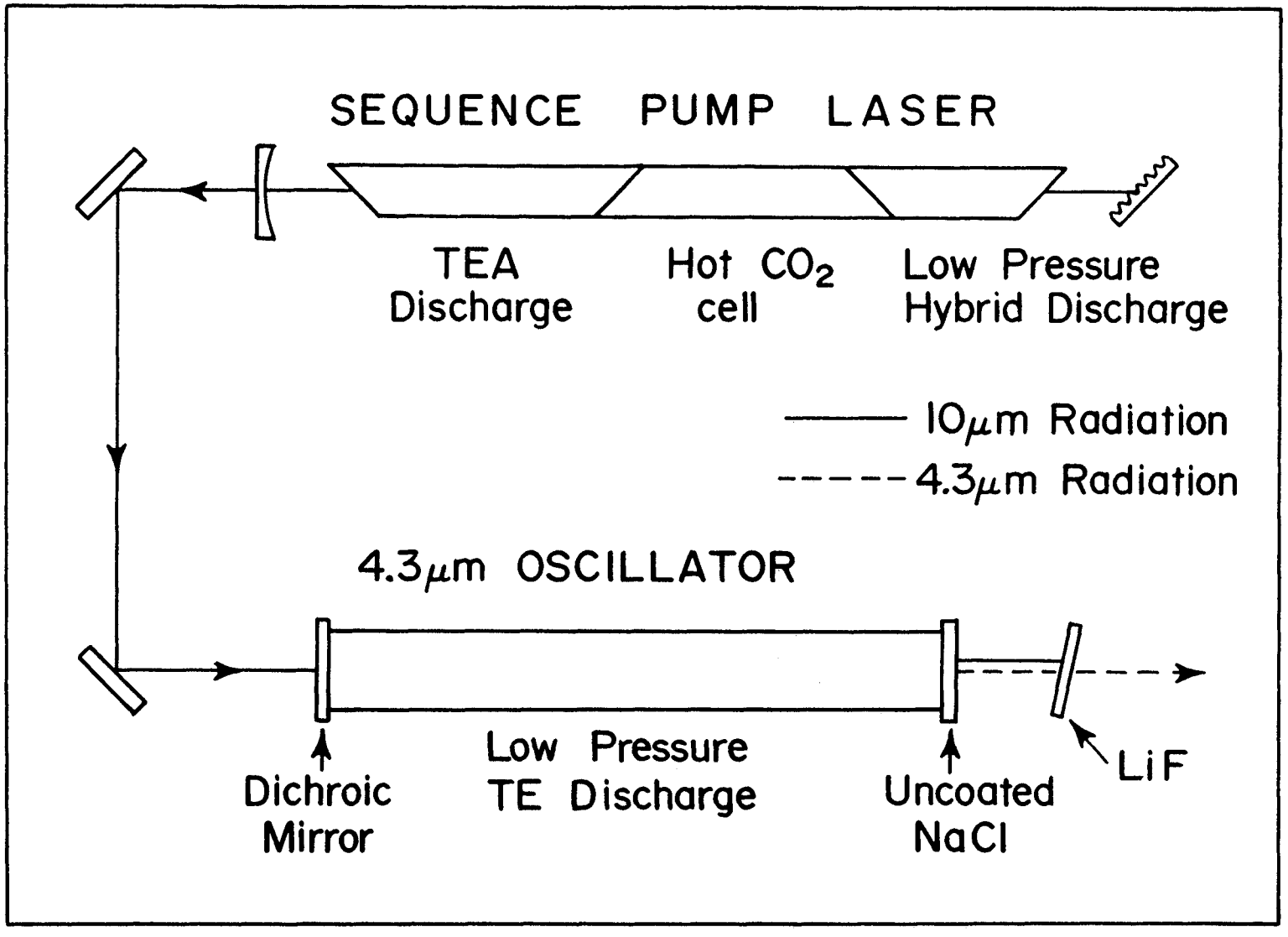
SEQUENCE PUMP LASER
TEA Discharge
Hot CO_2 cell
Low Pressure Hybrid Discharge
10μm Radiation
4.3μm Radiation
4.3μm OSCILLATOR
Dichroic Mirror
Low Pressure TE Discharge
Uncoated NaCl
LiF

and an uncoated NaCl flat serves as the output coupler of the 4.3 μm radiation. A LiF flat located near the output coupler absorbs the sequence pump radiation. The 145 cm-long low pressure discharge was operated at excitation energies of ~ 170 J/ℓ·atm with a flowing gas mixture (~ 3 ℓ/min NTP) of 4% CO_2 : 10% N_2 : 86% He at ~ 60 Torr. The 4.3 μm laser system was pulsed at 0.3 Hz and produced pulses with energies > 3 mJ on the P(17) to P(29) lines in the 10^01-10^00 band. Further details of the 4.3 μm laser are given elsewhere [6,46].

The probe laser consists of a 1 m-long (1 cm-bore) cw discharge and a 51 cm-long hot cell to allow operation on the sequence bands. The remainder of the 195 cm-long cavity consists of a 90% reflecting (10 μm) ZnSe output coupler mounted on a piezoelectric translator (PZT), and a Littrow-mounted PTR ML-304 original grating (135 lines/mm) with a measured 10 μm efficiency of > 97%. Flowing gas mixtures of 15% CO_2 : 15% N_2 : 70% He could be excited with maximum discharge currents of ~ 10 mA at pressures up to ~ 10 Torr. With the hot cell filled to ~ 20 Torr of CO_2 at a temperature of ~ 530 K, output powers of ~ 600 mW were obtained on the 9 μm P(19) line. With the cell evacuated, output powers of > 5 W were easily produced on the 9 μm P(18) line. Intra-cavity apertures at both ends of the cavity allowed oscillation only on the TEM_{00} mode.

The pump and probe beams are focussed into a waveguide cell by a 50 cm focal length BaF_2 lens and a 25 cm f.l. Ge lens respectively. The waveguide cell consists of a 1.3 mm-bore pyrex tube sealed with NaCl windows. The overall length of the cell was limited by the (strong)

absorption of the pump beam. For the dilute mixture measurements, a 4.9 cm-long pyrex tube resulted in a total cell length of 5.5 cm. (A 1.01 cm tube with an overall cell length of 1.09 cm was used in the high CO_2 content mixtures). Including the losses in the NaCl windows, approximately 65% of the pump beam and 85% of the probe beam were transmitted through the empty cell. At maximum pump power, the average pump fluence inside the empty cell was ~ 350 mJ/cm^2. Typical energy absorption coefficients were 10 %/cm even in dilute CO_2 mixtures. The total pressure was monitored by a 0-1000 Torr capacitance manometer (MKS Instruments Baratron #221AHS-A-1000) at the outlet of the cell. No pressure differential was observed between the inlet and the outlet. The waveguide cell can safely withstand pressures up to ~1000 Torr. Flowmeters calibrated to better than ± 5% accuracy were used to regulate the mixtures in the cell. The use of a waveguide cell has many advantages -- a high pump fluence can be maintained over moderate path lengths, good spatial overlap is ensured between the pump and probe beams, the cell volume (and hence the absorbed energy) are accurately known, and any deviation of the probe beam due to shock waves induced by the pump pulse is minimized.

After the cell, a second dichroic mirror and a cell containing pure CO_2 removed any residual pump radiation. Various highly reflecting 10 μm mirrors attenuated the probe beam to a safe level before it reached the detector. The signal falling on the fast Hg:Cd:Te detector (Infrared Associates #HCT-50 with risetime ~ 50 ns) was recorded on a Tektronix 468 storage oscilloscope interfaced to an IBM PC computer.

3.3 Experimental Technique

As the goal in this thesis was to attain as high a value of T_3 as possible, the absorbed energy per CO_2 molecule was maximized with the 4.3 μm laser transition, the pump intensity, the CO_2 content and the total pressure of the mixture. As a result, the 4.3 μm CO_2 laser was operated on the P(20) transition of the (10°1-10°0) band at 2310 cm^{-1}. Pulse energies of 9 mJ and pulse widths of ~ 75 ns FWHM with peak powers of 120 kW were obtained. The exact coincidence of this wavelength with the absorbing transition in the optically-pumped cell ensures that strong absorption will occur. In addition, overlapping absorptions from other ν_3 band transitions contribute significantly to the overall absorption in low CO_2 content mixtures at high pressure. As the pump energy is absorbed by the CO_2 in the waveguide cell, T_3 increases and additional transitions contribute to the overlapping absorptions. Detailed calculations and preliminary measurements confirm that the 4.3 μm absorption is not "bleached" at high input energy; on the contrary, the absorption can even increase slightly with increasing pump energy.

The experimental constraints described above result in a probe amplification of only a few percent per pass and necessitated the development of a sensitive technique for measuring transient gain. Gain measurements were generally made in two stages. The cw probe beam was mechanically chopped and the Hg:Cd:Te detector signal recorded to establish the cw baseline. The chopper was then stopped and the detector signal processed by a calibrated amplifier and high pass filter before recording the gain pulse. The gain factor of the amplifier (IRA

PPA C-086) was 406 ± 3% and was measured with the 9 μm P(18) probe signal. The purpose of the high pass RC filter (~ 90% transmitting for a 1 kHz sine wave) was to remove the low frequency oscillations of the cw baseline. No measurable difference was observed between gain signals with and without the filter in place. Care was taken to check the linearity of the detector and electronics. The two-stage measurement technique was later verified against a direct technique in which the gain pulse was recorded simultaneously with the chopped probe signal [38]. Both techniques agreed within experimental error.

The output power of the probe laser was maximized and stabilized with the PZT before each gain measurement and rechecked for stability after each measurement. Significant elecromagnetic noise and pickup were encountered in earlier experiments. These problems were eventually alleviated by shielding the entire detector, the digital scope and the computer as well as using heavily shielded BNC cables. Typical gain signals are shown in Fig. 3-3. Gains as low as 0.3 %/pass have been measured with reasonable signal-to-noise ratios. Typically, the limiting noise level is equivalent to less than 0.03 %/pass as can be seen from Fig. 3-3. At higher pump intensities, shock waves in the cell create periodic disturbances in the gain signal and affect the determination of the fall time of the gain. These disturbances do not affect the measurement of the gain peak. In general, peak gain coefficients can be measured with an accuracy of better than ± 5% and signals of the type shown in Fig. 3-3 are very reproducible from shot-to-shot. Day-to-day reproducibility is better than ± 10%.

FIGURE 3-3

Typical gain signals for the regular 9 μm P(18) and the sequence P(19) line as measured in a 1.4%CO_2 : 98.6%He mixture at a total pressure of 1027 Torr. In each case, 8 successive pulses are averaged. Some electrical noise is present before the arrival of the 4.3 μm pump pulse. The absorbed energy per unit volume was ~ 5 mJ/cc, and the pump pulse had a duration of < 200 ns.

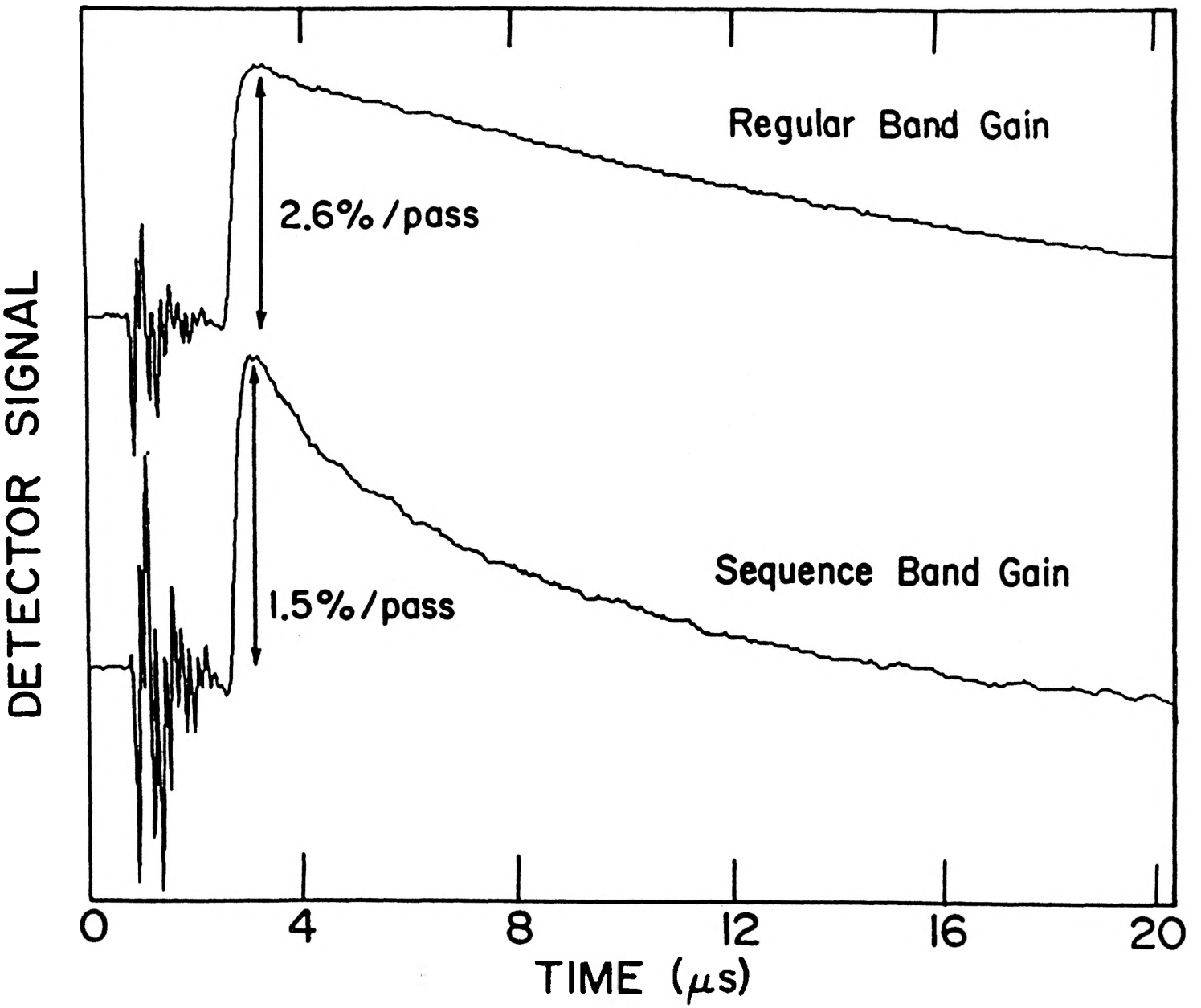
Regular Band Gain
2.6% /pass
Sequence Band Gain
1.5% /pass
DETECTOR SIGNAL
0
4
8
12
16
20
TIME (μs)

3.4 Summary

This chapter has presented the experimental technique used in measuring gain coefficients in optically-pumped CO_2 mixtures. The high sensitivity and good reproducibility of this technique allows one to accurately characterize optically-pumped CO_2 over a wide range of conditions. In the next chapter, a detailed study of the gain characteristics of CO_2 under high ν_3 mode excitation is discussed.

Chapter 4

GAIN MEASUREMENTS

4.1 Introduction

The measurement of gain coefficients in the low-lying levels of the ν_3 mode of CO_2 is presented in this chapter. In order to facilitate comparison with theory, measurements were first made in dilute CO_2 mixtures to ensure uniform pumping over the length of the cell. Then measurements were made in high-CO_2 content mixtures which were more representative of conventional CO_2 laser mixtures. Finally, an attempt to create lasing on the high-lying levels of the ν_3 mode is described.

4.2 Dilute Mixtures

4.2.1 Determination of Mode Temperatures

An optically-pumped CO_2 system is much easier to characterize than discharge-excited CO_2 systems as all the energy absorbed from the optical pulse goes directly into exciting the ν_3 mode of CO_2. There is no need to consider electron energy distributions, excitation efficiencies of the various modes or gas heating. As an example of the simplicity of the optically-pumped system, consider the case of a 2% CO_2 in He mixture at a total pressure of 1000 Torr pumped with a 4.3 μm fluence of 350 mJ/cm^2. Under these conditions, the collisional relaxation time of the ν_3 mode is ~ 10 μs [27,29], while the total

duration of the pump pulse is ~ 150 ns. Clearly, there is negligible decay of the ν_3 mode population during the pump pulse and all the absorbed energy can be considered to be stored in the ν_3 mode. Although a significant fraction of the absorbed photons initially populate the 10^01 level , fast relaxations of the type shown in (2-9) quickly couple the absorbed energy into the ν_3 mode. For a 2% CO_2 mixture at 1000 Torr, the time constant for this process is ~ 10 ns [24]. Similar fast collision processes couple levels within the ν_3 mode and ensure a Boltzmann distribution is established on a timescale of ~ 5 ns [21]. The rotational relaxation time is < 0.2 ns [18] and ensures the rotational levels also follow a Boltzmann distribution. Thus the energy stored in the ν_3 mode and hence the vibrational temperature T_3 can be simply determined from the measured 4.3 μm energy absorbed per unit volume.

To fully characterize the CO_2 medium after optical pumping, the other temperatures T_1, T_2 and T must also be known. Accurate techniques for determining these temperatures in discharges using a variety of 10 μm probe transitions have been developed [1]. However, in the present system, the CO_2 gas is initially at room temperature and all the absorbed energy goes directly into the ν_3 mode. Consequently, if measurements are made immediately after the pump pulse, T_1, T_2 and T must remain close to 300 K. Even if all the absorbed energy is converted into heat, the calculated temperature rise in the 2% CO_2 mixture is < 40 K under the most extreme pumping conditions. As described in the next section, measurements have been carried out to confirm that gas

heating can be neglected for dilute CO_2 : He mixtures.

In summary, by measuring the absorbed 4.3 μm energy per unit volume of gas, all the relevant mode temperatures of the CO_2 medium can be determined. This in turn allows one to accurately calculate the 9 and 10 μm gain on the regular and sequence bands immediately after the optical pulse. In the next section, good agreement is shown between calculated and measured gain coefficients over a wide range of experimental conditions.

4.2.2 Results and Comparison with Theory

Gas mixtures of 1.3% and 2.3% CO_2 in He at ~ 1000 Torr were confined in a 5.5 cm-long cell. The average pump absorption per pass was ~ 36% and ~ 48% respectively. A plot of the measured absorbed energy per unit volume, E_3, as a function of pump fluence is shown in Fig. 4-1. The measurements were made with a Scientech 36-0001 calorimeter placed after the cell. Direct comparisons were then made of output energy with and without the gas mixture in the cell. The main source of error in the measurements was the ± 10% shot-to-shot variation in the pump beam energy. The linear variation of absorbed energy with input energy indicates that the average absorption coefficient in the waveguide is independent of pump intensity, i.e., any "bleaching" of the directly-pumped transitions is compensated by an increase in overlapping absorption as T_3 increases. This behaviour agrees with model predictions and allows the determination of E_3 from the measurements of transmitted pump energy alone. This value of E_3 is then used to

FIGURE 4-1

Variation of the average absorbed pump energy E_3 with the transmitted pump fluence through the waveguide cell. The lines represent least squares fits to the experimental points and are constrained to pass through the origin.

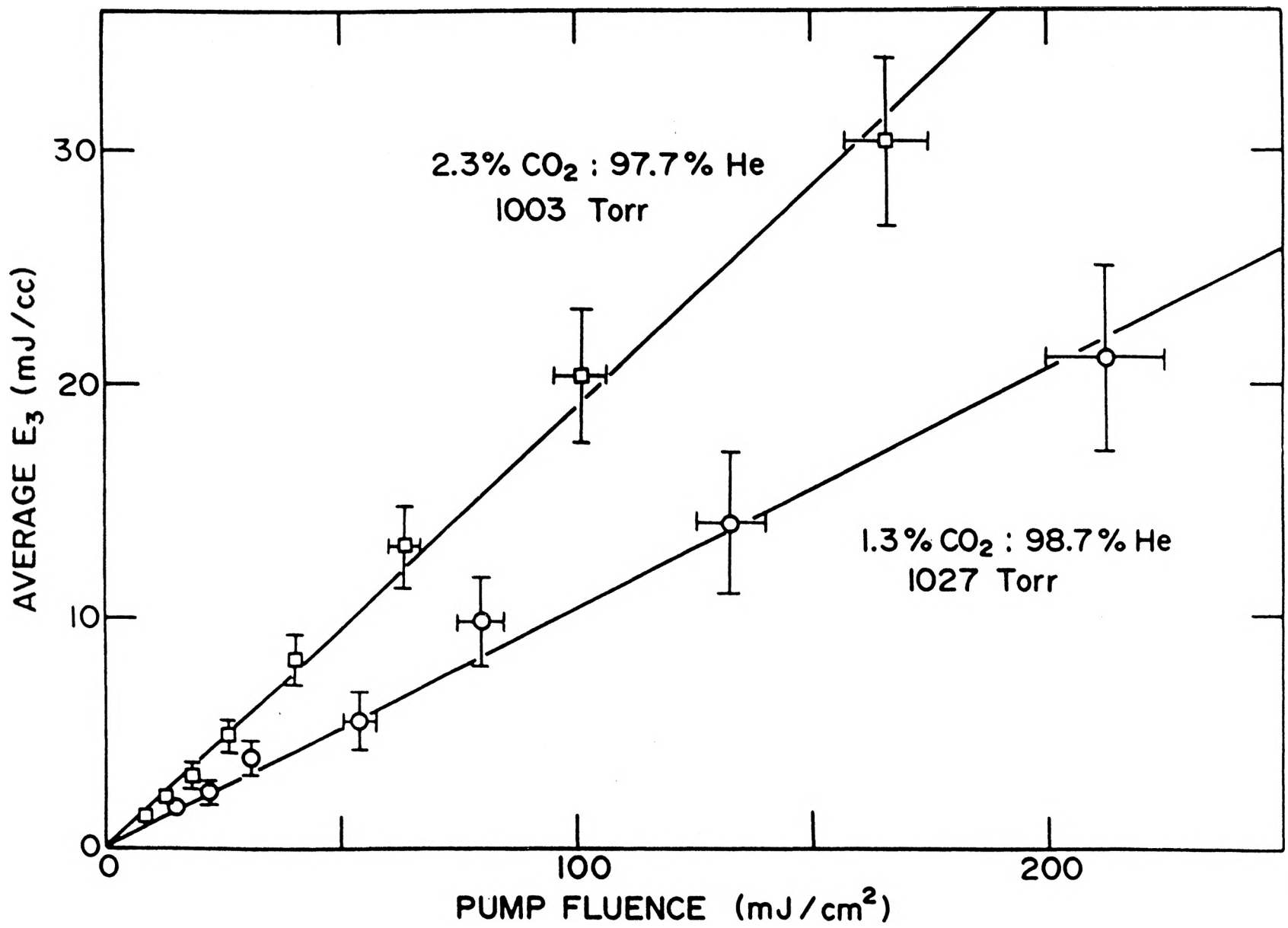
2.3% CO_2 : 97.7% He
1003 Torr
1.3% CO_2 : 98.7% He
1027 Torr
AVERAGE E_3 (mJ/cc)
PUMP FLUENCE (mJ/cm^2)
0
10
20
30
0
100
200

calculate T_3.

As explained in the previous section, the rotational/translational gas temperature is expected to remain close to room temperature after the 4.3 μm pulse. This assumption was checked by measuring gain in the 9.4 μm band as a function of rotational transition under conditions of high optical excitation. Results are shown in Fig. 4-2. The measured gain coefficients have been corrected for overlaps using the techniques of Ref. [1]. Five of the measured transitions had less than 10% additional gain from overlapping 9.4 μm transitions [1]; the P(34) and P(42) transitions required larger corrections. While the measurements of Fig. 4-2 do not allow an accurate determination of rotational temperature T, they are consistent with a $T \simeq 300$ K distribution (a similar calculation for T = 400 K results in a worse fit) and confirm that no systematic errors are present in the measurements of small amplifications of the probe beam.

At this point, the measured gain coefficients can be compared with the calculated values as a function of E_3. T_3 is determined from measurements of absorbed energy alone, while T_1 and T are assumed to remain equal to room temperature. Figure 4-3 shows such a comparison for a 1.4% CO_2 : 98.6% He mixture. Measurements are made on both regular and sequence transitions and overlapping gain contributions are included in the calculations. The 9 μm P(18) and P(19) lines were chosen as they had minimal overlap contributions.

In early modeling of the results, the vibrational temperature T_3 was determined from E_3 by assuming a Boltzmann distribution in the ν_3

FIGURE 4-2

Rotational gain distribution in the 9 μm regular P-branch measured at maximum pump power (E_3 ~ 24 mJ/cc). The measured transitions were chosen to minimize overlapping gain contributions from nearby transitions, and the data has been corrected for this overlapping gain (see text). The line represents the calculated gain distribution for T=293 K and is normalized to give a best fit.

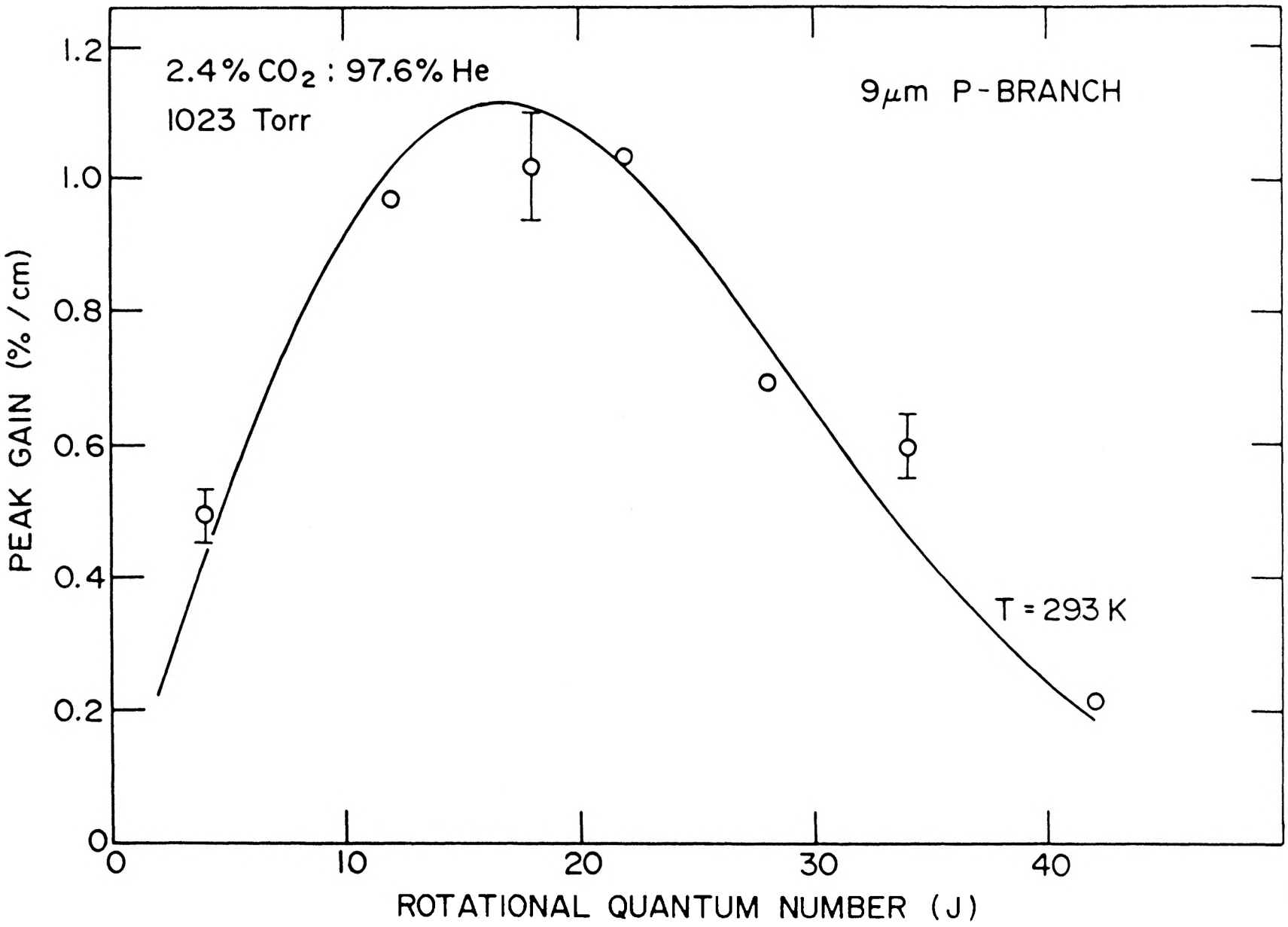
2.4% CO_2 : 97.6% He
1023 Torr
9μm P-BRANCH
T = 293 K
PEAK GAIN (% / cm)
ROTATIONAL QUANTUM NUMBER (J)
0
0.2
0.4
0.6
0.8
1.0
1.2
0
10
20
30
40

FIGURE 4-3

Variation of regular (O) and sequence (□) peak gain coefficients with optical energy absorbed in the gas. The dashed lines represent calculations based on a Boltzmann distribution and the solid lines represent those based on a Treanor distribution. Also shown are the variation of the Boltzmann temperature T_3 and the Treanor temperature T_3^* with the absorbed energy.

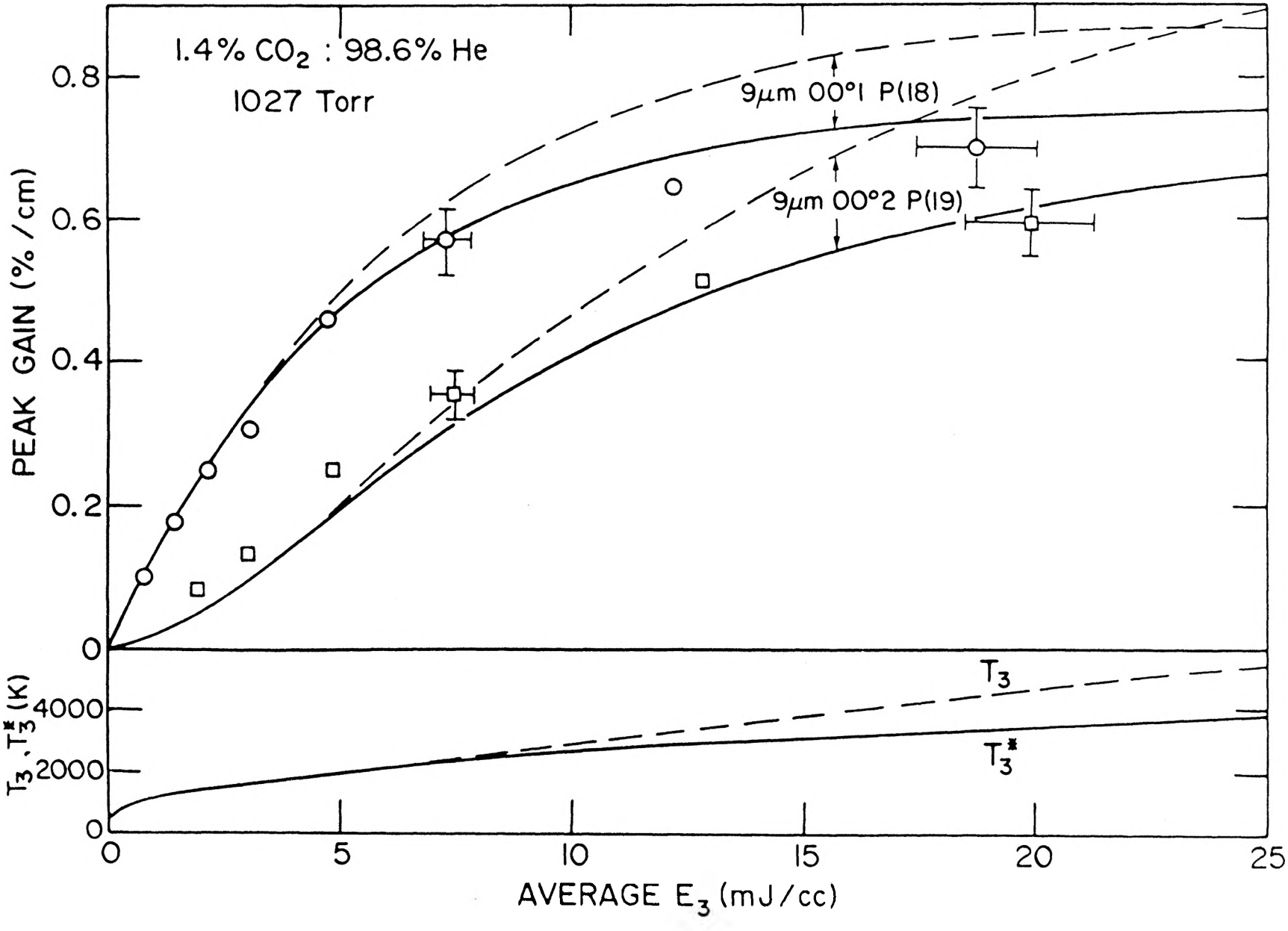
1.4% CO_2 : 98.6% He
1027 Torr
9μm 00°1 P(18)
9μm 00°2 P(19)
PEAK GAIN (%/cm)
0.8
0.6
0.4
0.2
0
T_3, T_3^* (K)
4000
2000
0
T_3
T_3^*
0
5
10
15
20
25
AVERAGE E_3 (mJ/cc)

mode population (See Eq. 2-20). Gain coefficients were then calculated for levels up to and including 00°9 using the computer model developed in [1]. All overlapping contributions to the P(18) and P(19) transitions were summed. In most cases, the overlapping contributions were < 9% of the P(18) and < 15% of the P(19) gain coefficients. As can be seen in Fig. 4-3, the calculations based on a Boltzmann distribution overestimate the gain coefficients at high input energy, particularly for the sequence transitions. It was then realized that the anharmonicity of the CO_2 molecule must be explicitly taken into account by using a Treanor distribution for the stored energy. (Previous measurements in cw discharges have shown that Treanor distributions accurately represent the energy distribution in the ν_3 mode [2]).

In a Treanor distribution (See Eq. 2-18), more energy is stored in the upper levels of the ν_3 mode than in a Boltzmann distribution. Therefore, for the same amount of ν_3 mode energy, the 00°2 and 00°1 populations and hence the regular and sequence band gain coefficients will be lower than those calculated with a Boltzmann distribution. To carry out calculations with a Treanor distribution, the Treanor temperature T_3* was deduced from the measured absorbed energy by using Eq. (2-21). With this value of T_3^*, gain calculations were carried out as before and are represented by the solid curves in Fig. 4-3. It is gratifying that the value of T_3^* determined solely from absorption measurements leads to calculated gain coefficients which are in good agreement with experiment.

Some further points can be made concerning the data presented in Fig. 4-3. At high pump energies, the P(19) gain coefficient is ~ 85% of that measured on the P(18) line. In some experiments with more dilute CO_2 mixtures, sequence band gain coefficients were measured to be almost equal to the regular band gain coefficients. This gain ratio is a very direct indication of high vibrational temperatures in the ν_3 mode. In contrast, discharge-excited CO_2 gain media rarely attain a gain ratio of greater than 50% [50]. The results shown in Fig. 4-3 also indicate that there is no saturation of the ν_3 mode excitation. All the absorbed pump energy is stored in the ν_3 mode in a Treanor distribution. However, the P(18) gain coefficient does level-off with increasing input energy. This "saturation" is caused by a form of overpumping of the ν_3 mode - additional input energy simply increases the populations in the 00°2, 00°3, 00°4, ... levels. This leveling-off of gain represents a real limitation on the maximum gain coefficient attainable in the 9.4 μm regular band.

Similar results are shown in Fig. 4-4 for a 2.3% CO_2 mixture. Note that the limiting gain coefficient on the P(18) transition, as calculated with the Treanor distribution, has approximately scaled with the CO_2 content of the mixture. The agreement between theory and experiment in Fig. 4-4 is not quite as good as in Fig. 4-3. The discrepancy in Fig. 4-4 is probably caused by variations of T_3^* along the waveguide as the pump beam is more strongly absorbed. (The model assumes a uniform T_3^* calculated from the average absorbed energy). Nevertheless, the data of Fig. 4-4 confirm that high vibrational

FIGURE 4-4

Variation of peak gain coefficient with E_3 for a 2.3% CO_2 mixture. See Figure 4-3 for further details.

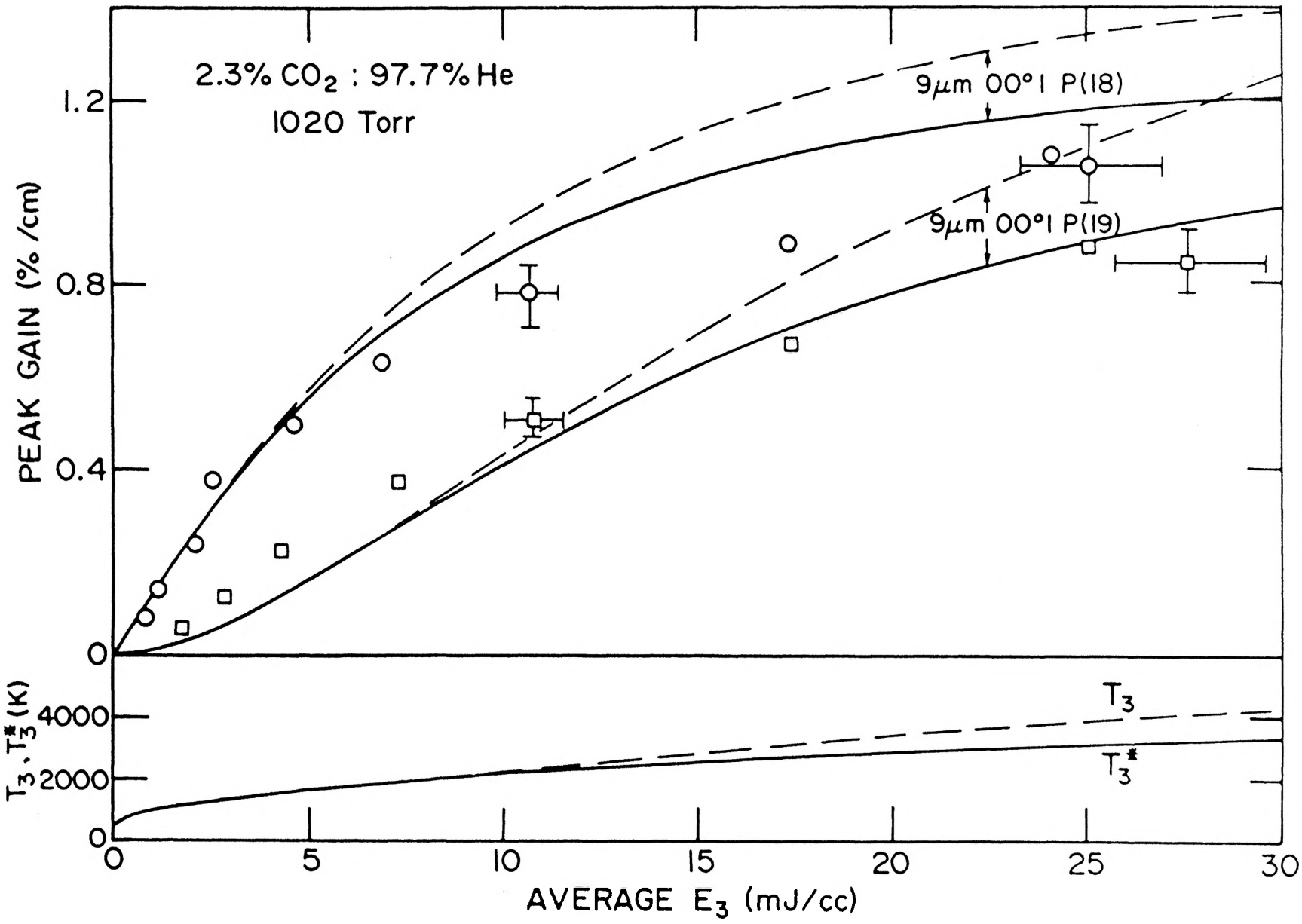
2.3% CO_2 : 97.7% He
1020 Torr
9μm 00°1 P(18)
9μm 00°1 P(19)
PEAK GAIN (% /cm)
1.2
0.8
0.4
0
T_3, T_3^* (K)
4000
2000
0
T_3
T_3^*
0
5
10
15
20
25
30
AVERAGE E_3 (mJ/cc)

temperatures are also attained in the 2.3% CO_2 mixture.

4.2.3 Gain Lifetimes

The transient gain profiles shown in Fig. 3-3 can also be used to determine relaxation rates. Fig. 4-5 plots the log of the decay of the regular and sequence band gain signals as derived from the traces in Fig. 3-3. A least squares fit to the data points gives regular and sequence relaxation times of 11.4 and 4.4 μs respectively, in satisfactory agreement with the calculated values of 11.5 and 5.8 μs [27,29]. (At low input energies, the sequence band decay time should be approximately half that of the regular band if the 00°1 and 00°2 levels are to maintain a Boltzmann distribution throughout their decay). At full pump energies and higher initial values of T_3^*, gain signals of the type shown in Fig. 4-6 are obtained. Both regular and sequence band gain profiles comprise an early fast relaxation followed by the conventional relaxation of a Boltzmann distribution towards thermal equilibrium. This accelerated relaxation rate at high T_3^* has been previously predicted for molecules such as N_2 [15]. In CO_2, it appears that fast V-T relaxation reduces E_3 when the high-lying vibrational levels are significantly populated. As T_3 decreases towards the values obtained in more conventional excitation schemes, the normal relaxation process of the ν_3 mode dominates. More study is required to investigate this fast relaxation of CO_2 at high values of E_3.

FIGURE 4-5

Semi-log plots of the decay rates of the regular and sequence gain signals as derived from Figure 3-3. Time is measured from the peak of the gain pulses and a linear least squares fit to the data is also shown. The relative error in the calculated relaxation rates is ± 20%.

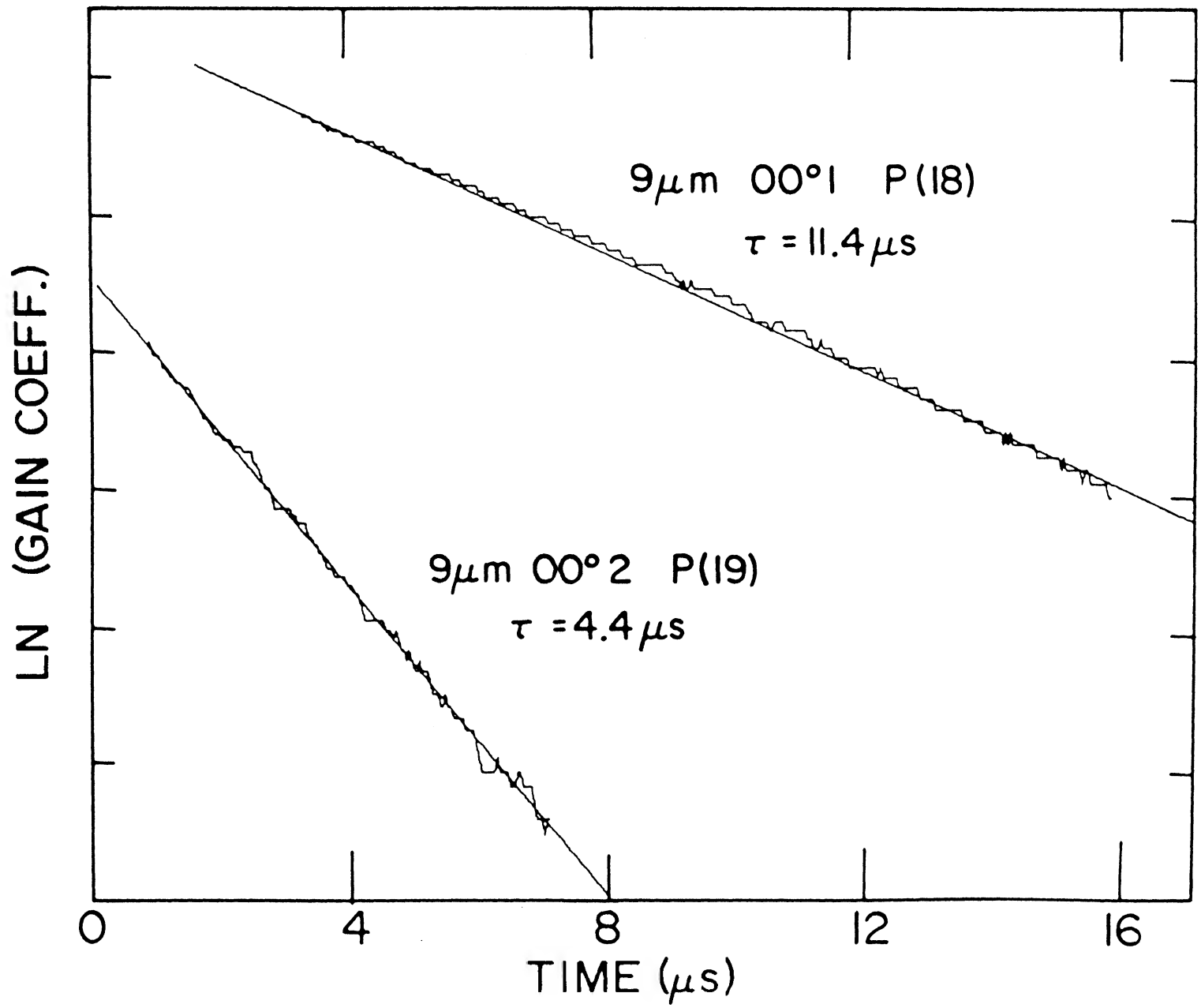
9μm 00°1 P(18)
τ = 11.4 μs
9μm 00°2 P(19)
τ = 4.4 μs
LN (GAIN COEFF.)
0
4
8
12
16
TIME (μs)

FIGURE 4-6

Gain signals on the regular and sequence bands measured under conditions similar to those in Figure 3-3, but at maximum pump power. The absorbed E_3 was ~ 20 mJ/cc. Note the fast relaxation at the beginning of the decay and the presence of shock waves in the tail.

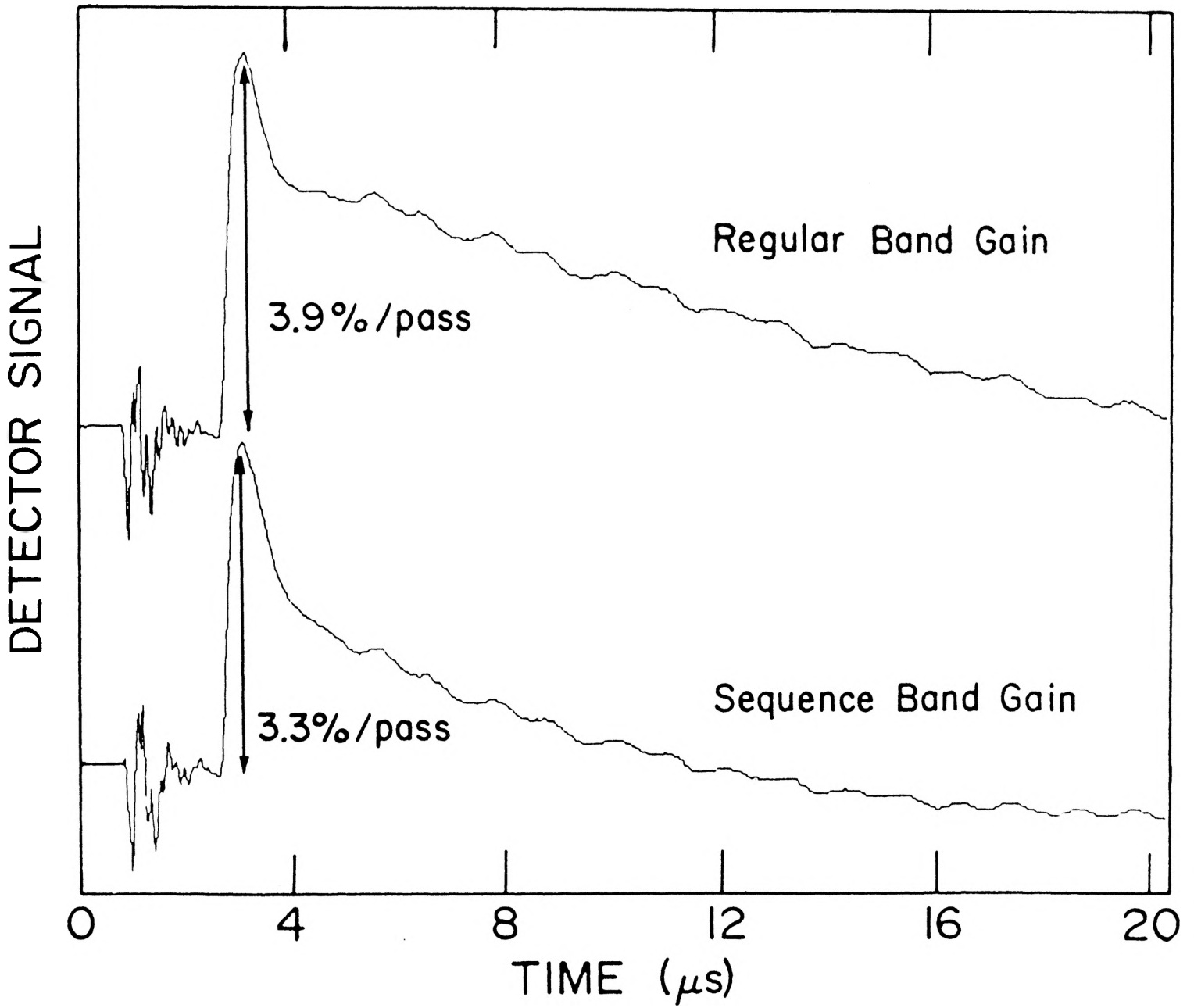
DETECTOR SIGNAL
Regular Band Gain
3.9%/pass
Sequence Band Gain
3.3%/pass
0
4
8
12
16
20
TIME (μs)

4.3 High-CO_2 Content Mixtures

In view of the high vibrational temperatures achieved in dilute mixtures, it was decided to investigate more conventional CO_2 laser mixtures. Due to the strong absorption of the pump beam, a 1.09 cm-long waveguide cell was used. The measurement technique was identical to the one used previously and many of the gain measurements were confirmed by using a direct method [38]. This method uses a He-Ne laser and a repetition rate control unit to synchronize the firing of the 4.3 μm laser so that the transient gain pulse is superimposed on the chopped probe signal (See Fig. 4-7). Gain measurements were made on 40% CO_2 : 60% He mixtures and pure CO_2 at ~ 300 Torr. In general, the measurements were performed with approximately 1/4 of the full pump energy to limit gas heating. At high CO_2 concentration, the energy stored in the ν_3 mode produces severe heating as it decays by V-T collisional processes. This heating speeds up the V-T relaxation process [27,29] and results in very short gain pulses at high pump energy. In addition, for pure CO_2 , the relaxation rates of the ν_3 mode and the 01^10 level are comparable and the 9 μm lower level becomes significantly populated during the relaxation process.

Despite these problems with short lifetime of the gain, peak gain coefficients have been measured in optically-pumped CO_2 which are substantially higher than those measured in discharge-excited CO_2. Table 4-1 gives typical results. Due to the overlapping 9 μm R(17) 00°2 transition, the gain on 9 μm R(12) is often greater than the gain on 10 μm P(20) [51]. The values in Table 4-1 should be contrasted with the

FIGURE 4-7

Typical 10 μm P(20) gain signal superimposed on the chopped probe beam as measured in 320 Torr of CO_2. The displayed gain signal with a 2.5 μs FWHM represents a gain coefficient of ~ 17 %/cm over the 1.09 cm-long waveguide cell. The absorbed energy per unit volume was ~ 45 mJ/cc.

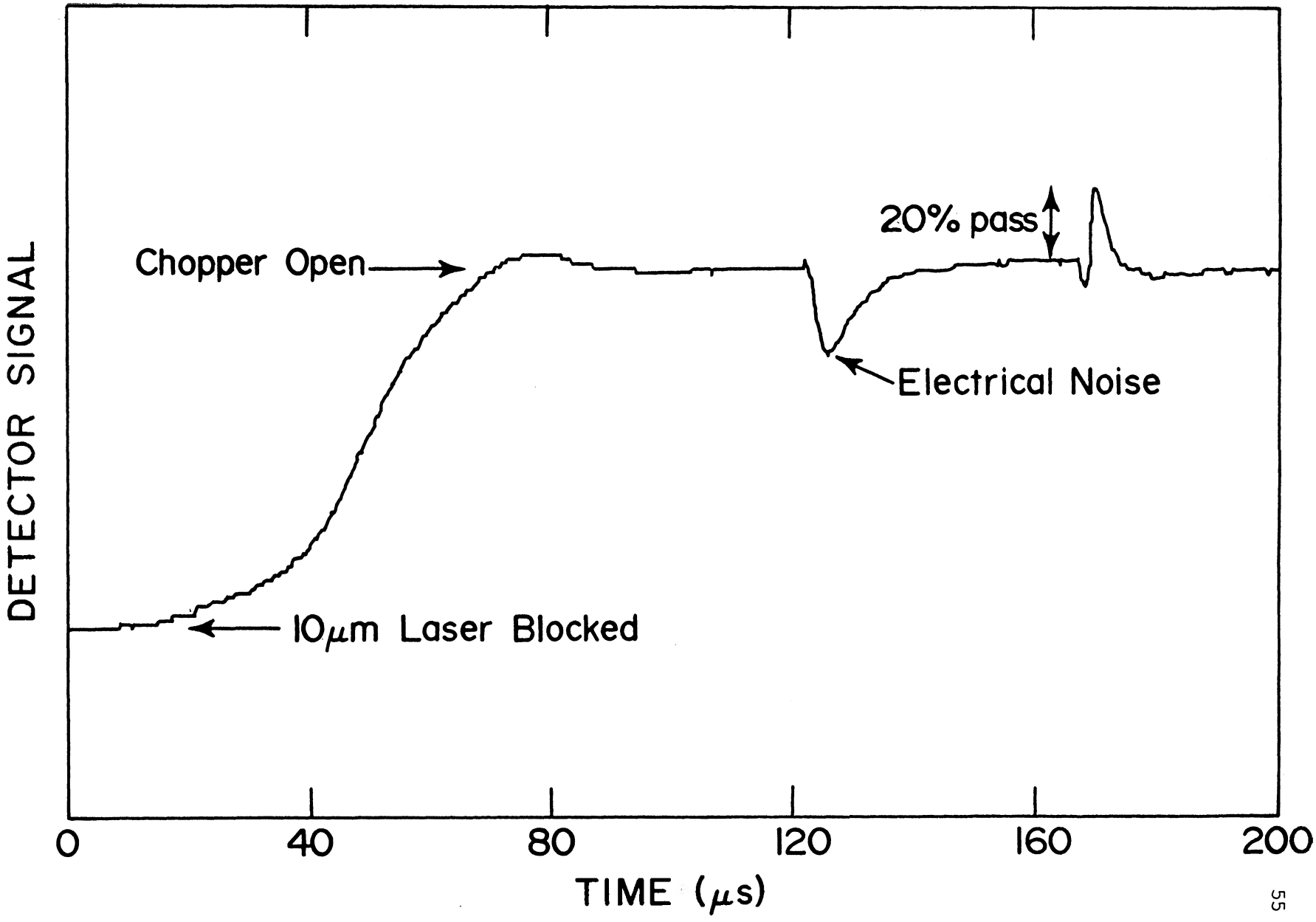
DETECTOR SIGNAL
Chopper Open
20% pass
Electrical Noise
10μm Laser Blocked
0
40
80
120
160
200
TIME (μs)

TABLE 4-1

Measured gain coefficients in CO_2 mixtures at 300 Torr. The absorbed pump energy was ~ 20 mJ/cc in the 40% CO_2 mixture and ~ 45 mJ/cc in pure CO_2.

Mixture	Peak Gain Coefficient (%/cm)		
CO_2:He	10 μm P(20)	9 μm R(12)	9 μm P(19)
0.4 : 0.6	10	10	3.6
1.0 : 0.0	17	20	5.5

optimum values of 5 %/cm regular and ~1 %/cm sequence band gain coefficients attained in conventional TE CO_2 discharges [8,52].

4.4 Treanor Laser

A consequence of a Treanor distribution with a high value of T_3^* is the prediction of partial inversion in the (00°n-00°(n-1)) bands. This type of inversion mechanism accounts for the operation of CO lasers. Computer calculations indicate that in a 1.4% CO_2 mixture, partial inversion should occur for bands with n > 6 and that gain coefficients of ~ 2 %/cm should be attained in the (00°9-00°8) band at 4.7 μm.

The configurations used in attempting 4.7 μm lasing were very similar to the double resonance experiments. In the first attempt, a CO laser output coupler (~ 54% transmitting at 4.3 μm P(20)) was used to couple in the pump radiation. Another CO output coupler (> 99% reflecting at 4.3 μm P(20)) formed the other end of the 8.7 cm-long waveguide cavity. Both mirrors were placed in special adapters which were mounted directly onto the cell. These adapters limited the maximum operating pressure to ~ 1 atm. Unfortunately, no lasing at 4.7 μm was observed even when the waveguide was cooled with dry ice. (An examination of the expression for the Treanor distribution (Eq. 2-18) shows that higher populations in the upper ν_3 levels can be achieved by lowering T).

In the second attempt, the 4.3 μm radiation was coupled into the cavity with a grating. The waveguide was replaced with an aluminum tube

sealed with Brewster Nacl windows. A PTR ML-402-12 replica grating (300 lines/mm) blazed at 5.4 μm and a gold mirror (f.l. = 15 cm) formed the rest of the 10 cm-long cavity. Again, no lasing was observed over a wide range of CO_2 mixtures and pressures.

The absence of 4.7 μm lasing may be explained by the existence of fast V-T relaxation processes from the upper levels, as indicated in Fig. 4-6, which may preclude the generation of partial inversion in CO_2 [15]. However, in view of the potential applications of a laser operating in the 4.5-4.9 μm region, it may be worth repeating this type of experiment with an HF laser as the pump source. The HF laser can pump directly from the ground state of CO_2 into the 10^01 level [53].

4.5 Summary

The experiments in this chapter have shown that higher ν_3 mode gain coefficients and vibrational temperatures are achieved in optically-pumped CO_2 than in discharge-excited CO_2. If, for comparison purposes only, one assumes that the ν_3 mode Boltzmann temperature T_3 is given by [1],

$$(g_{seq} / g_{reg})_{9\mu m} = 1.89 \exp(-h\nu_3/kT_3) \qquad (4\text{-}1)$$

then the results of Figs. 4-3 and 4-4 give T_3 values of ~ 4200 K at the highest input energies. In contrast, the maximum value of T_3 attained in conventional discharges for 1 to 2% CO_2 mixtures is ~ 3100 K [6]. Furthermore, the discharge-excited systems required the addition of N_2 in the mixture; in the absence of N_2, the T_3 value is ~ 1800 K for dilute

CO_2 mixtures in He [5]. In the optically-pumped system, the addition of N_2 had very little effect upon the value of T_3.

The good agreement obtained between experimental and calculated gain confirms the validity of a Treanor population distribution in the ν_3 mode. An accelerated relaxation rate, which is one of the features of a Treanor distribution with a high T_3^*, was observed. The existence of a partial inversion in high-lying ν_3 mode levels, also predicted by the Treanor model, cannot be confirmed due to the failure to observe lasing on these bands. More study is required to understand the characteristics of the upper levels of a Treanor distribution, especially in regard to V-T decay rates, which may have been responsible for suppressing any lasing action on these bands.

Chapter 5

CONCLUSIONS

This study has demonstrated that optical pumping of CO_2 at 4.3 μm can produce a higher excitation of the ν_3 mode (and therefore higher gain and T_3) than can electron excitation. It is believed that the difference between optical- and discharge-pumping is caused by the presence of electron de-excitation in a discharge. This de-excitation mechanism leads to a saturation in T_3 as the input energy increases. This work has shown that no such saturation occurs with optical pumping and that very high values of T_3 can be attained. At high values of T_3, the anharmonicity of the CO_2 molecule must be taken into account and the population in the ν_3 mode described by a Treanor distribution with a temperature T_3^*. As discussed in Chapter 4, this distribution results in an upper limit for the gain attainable on the 9 and 10 μm regular bands of CO_2. The gain measurements made in this study are close to this theoretical limit for dilute CO_2 mixtures. A similar calculation can be carried out for more conventional CO_2 laser mixtures. For example, a 20% CO_2 : 80% He mixture with $T_1 = T_2 = 300$ K and a ν_3 mode temperature T_3^* of 3500 K will have a theoretical gain limit of ~ 10 %/cm on the 9 μm P(18) transition. (This maximum gain scales approximately linearly with CO_2 content in the range 5 to 50% and gain coefficients are 10 to 20% higher in the 10 μm band). To our

knowledge, discharge-excited CO_2 systems have never produced gain coefficients close to this theoretical limit. High gain coefficients have been attained by excitation techniques which avoid electron de-excitation [54,55].

At high excitation energies of the ν_3 mode, it was discovered that the regular and sequence gain coefficients decayed at accelerated rates. This feature is characteristic of a Treanor distribution with a high value of T_3^*. The existence of partial inversions in the upper levels of the ν_3 mode at high T_3^* could not be confirmed. Further studies are required to fully understand the gain dynamics of the high-lying levels of the ν_3 mode.

An interesting extension of the measurements made in this study is to optically pump high pressure CO_2 (>> 1 atm) at 4.3 μm. At sufficiently high pressure (> 15 atm), the individual gain linewidths broaden to form a continuous band and continuously tunable operation should be possible from 9 to 11 μm. The absence of electron de-excitation in optical pumping should result in higher gains and energy extraction than that is attainable in multi-atmosphere CO_2 discharge lasers. A more fundamental question, however, arises from the results in this study. Although regular band gain coefficients close to the theoretical limit have been achieved, the ν_3 mode vibrational temperature has not shown any evidence of saturation with excitation energy. It should prove interesting to determine if T_3 can continue to increase to the point of dissociation. If this is true, then it may be possible to create CO_2 lasing in the upper ν_3 mode levels using the same

anharmonic pumping scheme as that employed in CO lasers. In addition, a detailed study of the population distribution of the ν_3 mode under high excitation (especially in the upper levels) will provide much needed insight in this area.

In summary, the first detailed gain measurements in optically-pumped CO_2 have been reported in this study. These experiments have demonstrated that high vibrational temperatures and gain coefficients can be achieved in the absence of electron de-excitation which limits the performance of discharge-excited CO_2 lasers.

REFERENCES

1. R.K. Brimacombe and J. Reid, "Measurements of Anomalous Gain Coefficients in Transversely Excited CO_2 Lasers," IEEE J. Quantum Electron. OE-19, 1674-1678 (1983).

2. C. Dang, J. Reid, and B.K. Garside, "Detailed Vibrational Population Distributions in a CO_2 Laser Discharge as Measured with a Tunable Diode Laser," Appl. Phys. B 27, 145-151 (1982).

3. B.F. Gordietz, N.N. Sobolev, V.V. Sokovikov, and L.A. Shelepin, "Population Inversion of the Vibrational Levels in CO_2 Lasers," IEEE J. Quantum Electron. OE-4, 796-802 (1968).

4. C.B. Moore, R.E. Wood, B.-L. Lu, and J.T. Yardley, "Vibrational Energy Transfer in CO_2 Lasers," J. Chem. Phys. 46, 4222-4231 (1967).

5. C. Dang, J. Reid and B.K. Garside, "Gain Limitations in TE CO_2 Laser Amplifiers," IEEE J. Quantum Electron. OE-16, 1097-1103 (1980).

6. R.K. Brimacombe, J. Reid, and T.A. Znotins, "Gain Dynamics of the 4.3 μm CO_2 Laser," Appl. Phys. B 36, 115-124 (1985).

7. K.J. Siemsen, J. Reid, and C. Dang, "New Techniques for Determining Vibrational Temperatures, Dissociation, and Gain Limitations in cw CO_2 Lasers," IEEE J. Quantum Electron. OE-16, 668-676 (1980).

8. C.A. Fenstermacher, W.T. Leland, M.J. Nutter, J.P. Rink, and K. Boyer, "Parametric Studies of the Electron-Beam-Controlled Discharge IN CO_2 Laser Media," IEEE J. Quantum Electron. OE-8, 596 (1972).

9. A.L.S. Smith and J. Mellis, "Operating Efficiencies in Pulsed CO_2 Lasers," Appl. Phys. Lett. 41, 1037-1039 (1982).

10. C. Dang, J. Reid, and B.K. Garside, "Dynamics of the CO_2 Upper Laser Level as Measured with a Tunable Diode Laser," IEEE J. Quantum Electron. OE-19, 755-764 (1983).

11. A.R. Davies, "Calculations on Output Pulse Shapes, Gain Pulse Profiles, and Gain Limitation in the CO_2 TEA Laser," J. Appl. Phys. 47, 2037-2043 (1976).

12. V.V. Nevdakh, "Vibrational Temperatures and Gain Limitation in CO_2 Lasers," Infrared Phys. 25, 743-749 (1985).

13. T.Y. Chang and O.R. Wood, "Optically Pumped Continuously Tunable High-pressure Molecular Lasers," IEEE J. Quantum Electron. OE-13, 907-915 (1977) and cited references.

14. C.E. Treanor, J.W. Rich, and R.G. Rehm, "Vibrational Relaxation of Anharmonic Oscillators with Exchange-dominated Collisions," J. Chem. Phys. 48, 1798-1807 (1968).

15. G.E. Caledonia and R.E. Center, "Vibrational Distribution Functions in Anharmonic Oscillators," J. Chem. Phys. 55, 552-561 (1971).

16. R.K. Brimacombe, "4.3 μm TE CO_2 Laser Dynamics," Ph.D. Thesis, McMaster University, 1984.

17. G. Herzberg, Infrared and Raman Spectra (Van Nostrand, New York, 1945).

18. R.R. Jacobs, K.J. Pettipiece, and S.J. Thomas, "Rotational Relaxation Rate Constants for CO_2," Appl. Phys. Lett. 24, 375-377 (1974).

19. R.L. Abrams and P.K. Cheo, "Collisional Relaxation of CO_2 Rotational Levels by N_2 and He," Appl. Phys. Lett. 15, 177-178 (1969).

20. M.D. Thomason, "Rapid Vibrational and Rotational Energy Transfer Rates in Heated Carbon Dioxide Collisions by Double Resonance Laser Spectroscopy," Ph.D. Thesis, University of Virginia, (Los Alamos National Laboratory:LA-9420-T, 1982).

21. R.T. Pack, "Analytic Estimation of Almost Resonant Molecular Energy Transfer due to Multipolar Potentials. VV Processes Involving CO_2," J. Chem. Phys. 72, 6140-6152 (1980).

22. L. Doyennette, M. Margottin-Maclou, A. Chakroun, H. Gueguen, and L. Henry, "Vibrational Energy Transfer from the (00°1) Level of $^{14}N_2O$ and $^{12}CO_2$ to the (m,n^l,1) Levels of these Molecules and their Isotopic Species," J. Chem. Phys. 62, 440-447 (1975).

23. I. Burak, Y. Noter, and A. Szoke, "Vibration-Vibration Energy Transfer in the ν_3 Mode of CO_2," IEEE J. Quantum Electron. QE-9, 541-544 (1973).

24. J. Finzi and C.B. Moore, "Relaxation of CO_2(10°1), CO_2(02°1), and N_2O(10°1) Vibrational Levels by Near-Resonant V→V Energy Transfer," J. Chem. Phys. 63, 2285-2288 (1975).

25. W.A. Rossner,Jr., A.D. Wood, and E.T. Gerry, "Deactivation of Vibrationally Excited Carbon Dioxide (ν_3) by Collisions with Carbon Dioxide or with Nitrogen," J. Chem. Phys. 50, 4996-5008 (1969).

26. C. Dang, J. Reid, and B.K. Garside, "Dynamics of the CO_2 Lower Laser Levels as Measured with a Tunable Diode Laser," Appl. Phys. B 31, 163-172 (1983).

27. F. Lepoutre, G. Louis, and H. Manceau, "Collisional Relaxation in CO_2 Between 180 K and 400 K Measured by the Spectrophone Method," Chem. Phys. Lett. 48, 509-514 (1977).

28. J. Taine and F. Lepoutre, "A Photoacoustic Study of the Collisional Deactivation of the First Vibrational Levels of CO_2 by N_2 and CO," Chem. Phys. Lett. 65, 554-558 (1979).

29. F. Lepoutre, G. Louis, and J. Taine, "A Photoacoustic Study of Intramolecular Energy Transfer in CO_2 Deactivated by Moatomic Gases Between 153 and 393 K," J. Chem. Phys. 70, 2225-2235 (1979).

30. L.A. Weaver, L.H. Taylor, and L.J. Denes, "Rotational Temperature Determinations in Molecular Gas Lasers," J. Appl. Phys. 46, 3951-3958 (1975).

31. W.T. Leland, M.J. Kircher, M.J. Nutter, and G.T. Schappert, "Rotational Temperature in a High-Pressure Pulsed CO_2 Laser," J. Appl. Phys. 46, 2174-2176 (1975).

32. D. Bailly, R. Farrenq, G. Guelachvili, and C. Rossetti, "$^{12}C^{16}O_2$ Analysis of Emission Fourier Spectra in the 4.5 μm Region: Rovibrational Transitions $0v_2^1v_3-0v_2^1(v_3-1)$, $v_2=1$," J. Mol. Spectrosc. 90, 74-105 (1981).

33. D. Bailly, R. Farrenq, and C. Rossetti, "Vibrational Luminescence of CO_2 Excited by DC Discharge," J. Mol. Spectrosc. 70, 124-133 (1978).

34. A. Baldacci, V.M. Devi, D.-W. Chen, and K.N. Rao, "Absorption Spectrum of CO_2 at 4.3 μm," J. Mol. Spectrosc. 70, 143-159 (1978).

35. L.S. Rothman and L.D.G. Young, "Infrared Energy Levels and

Intensities of CO_2 -II," J. Quant. Spectrosc. Radiat. Transfer 25, 505-524 (1981).

36. J.C. Polanyi, "Vibrational-Rotational Population Inversion," Appl. Opt. Suppl. 2, 109-127 (1965).

37. S.R. Drayson, "Rapid Computation of the Voigt Profile," J. Quant. Spectrosc. Radiat. Transfer 16, 611-614 (1976).

38. R.K. Brimacombe and J. Reid, "Accurate Measurements of Pressure-Broadened Linewidths in a Transversely Excited CO_2 Discharge," IEEE J. Quantum Electron. QE-19, 1668-1673 (1983).

39. R.T. Pack, "Pressure Broadening of the Dipole and Raman Lines of CO_2 by He and Ar. Temperature Dependence," J. Chem. Phys. 70, 3424-3433 (1979).

40. G. Yamamoto, M. Tanaka, and T. Aoki, "Estimation of Rotational Line Widths of Carbon Dioxide Bands," J. Quant. Spectrosc. Radiat. Transfer 9, 371-382 (1969).

41. V. M. Devi, B. Fridovich, G.D. Jones, and D.G.S. Snyder, "Diode Laser Measurements of Strengths, Half-Widths, and Temperature Dependence of Half-Widths for CO_2 Spectral Lines near 4.2 μm," J. Mol. Spectrosc. 105, 61-69 (1984).

42. G.L. Tettemer and W.G. Planet, "Intensities and Pressure-Broadened Widths of CO_2 R-Branch Lines at 15 μm from Tunable Laser Measurements," J. Quant. Spectrosc. Radiat. Transfer 24, 343-345 (1980).

43. J. Reid and K. Siemsen, "Laser Power and Gain Measurements on the Sequence Bands of CO_2," J. Appl. Phys. 48, 2712-2717 (1977).

44. R.K. Brimacombe, J. Reid, and T.A. Znotins, "Multi-Joule Pulses from a Sequence Band Transversely Excited Atmospheric CO_2 Laser," Appl. Phys. Lett. 39, 302-304 (1981).

45. T.A. Znotins, J. Reid, B.K. Garside, and E.A. Ballik, "4.3 μm TE CO_2 Laser," Opt. Lett. 4, 253-255 (1979).

46. R.K. Brimacombe and J. Reid, "15-mJ Pulses from a 4.3 μm CO_2 Laser," Appl. Phys. Lett. 45, 813-815 (1984).

47. O.R. Wood and T.Y. Chang, "Transverse-Discharge Hydrogen Halide Lasers," Appl. Phys. Lett. 20, 77-79 (1972).

48. P. Arrowsmith, J.C. Polanyi, H.H. Telle, and B. Yang, "Short-Cavity Hydrogen-Halide Laser," Appl. Opt. 22, 2716-2720 (1983).

49. H.N. Rutt, "A High-Energy Hydrogen Bromide Laser," J. Phys. D 12, 345-353 (1979).

50. T.A. Znotins, J. Reid, and R.K. Brimacombe, "Design of Efficient Transversely Excited Sequence CO_2 Lasers," J. Appl. Phys. 53, 2843-2850 (1982).

51. J. Reid and K.J. Siemsen, "Gain of High-Pressure CO_2 Lasers," IEEE J. Quantum Electron. QE-14, 217-220 (1978).

52. P. Lavigne, J.-L. Lachambre, and G. Otis, "Gain Measurements on the Sequence Bands in a TEA-CO_2 Amplifier," J. Appl. Phys. 49, 3714-3718 (1978).

53. Z. Drozdowicz, R.I. Rudko, S.J. Linhares, and B. Lax, "High Gain 4.3-4.3 μm Optically Pumped CO_2 Laser," IEEE J. of Quantum Electron. QE-17, 1574-1580 (1981).

54. H. Hara and A. Fujisawa, "High-Gain CO_2 Laser," Appl. Phys. Lett. 38, 65-66 (1981).

55. H. Hara, "Performance of a N_2/CO_2 Mixing Laser by Using a Rapid Mixing Technique," J. Appl. Phys. 52, 4959-4961 (1981).